Geochronology and geochemistry of late Jurassic adakitic intrusions and associated porphyry Mo–Cu deposit in the Tongcun area, east China: Implications for metallogenesis and tectonic setting

Yanwen Tang [a,*], Xiaofeng Li [a,b], Yuling Xie [c], Liang Liu [a], Tingguang Lan [a], Sebastien Meffre [d], Cheng Huang [a]

[a] State Key Laboratory of Ore Deposit Geochemistry, Institute of Geochemistry, Chinese Academy of Sciences, Guiyang 550081, China
[b] Key Laboratory of Mineral Resources, Institute of Geology and Geophysics, Chinese Academy of Sciences, Beijing 100029, China
[c] School of Civil and Environmental Engineering, University of Science and Technology Beijing, Beijing 100083, China
[d] CODES ARC Centre of Excellence in Ore Deposits, University of Tasmania, Hobart, TAS 7001, Australia

ARTICLE INFO

ABSTRACT

The genesis of adakites and associated Mo–Cu mineralization in non-arc settings in China is poorly constrained. Here, we present geochronology, geochemistry and Sr–Nd–Pb isotopes for the Tongcun intrusive complex, and report Pb isotopes and $^{40}Ar–^{39}Ar$ age for the Tongcun Mo–Cu deposit. The Tongcun intrusive complex is composed mainly by granodiorite and monzogranite (phase 1 and phase 2), with emplacement age of 160 Ma to 148 Ma. The Tongcun complex can be classified as typical high–K calc–alkaline I-type granitoid and also shows adakitic geochemical features. Moreover, the negative Nb, Ta, Ti, and P anomalies and enriched initial $^{87}Sr/^{86}Sr$ ratios of 0.7083–0.7092 of the Tongcun intrusive complex are consistent with those of the subduction–related magmatism. The $^{40}Ar–^{39}Ar$ dating of sericite, which is intergrown with chalcopyrite, indicates that the late Cu mineralization event occurred at ~155.5 Ma. The early Mo (Cu) and the late Cu mineralization events in this deposit were temporally, spatially and genetically associated with the emplacement of monzogranite (phase 1). There are no obvious linear correlation between SiO_2 and most of the major and trace elements, and all rock samples fall within the fields of unfractional crystallization felsic granites in $Zr + Nb + Ce + Y$ versus FeO^T/MgO and $(K_2O + Na_2O)/CaO$ diagrams, indicating that partial melting rather than fractional crystallization has played an important role for the formation of the Tongcun intrusive complex. Magmatic inherited zircons from the Tongcun granitoids with the age peaked at 780–812 Ma, imply that the Neoproterozoic igneous rocks in the lower crust have been incorporated into the magma source. The uniform $\varepsilon_{Nd}(t)$ (−6.3 to −7.3), initial $^{87}Sr/^{86}Sr$, $^{207}Pb/^{204}Pb$ (15.596–15.621), and $^{208}Pb/^{204}Pb$ (38.374–38.650), as well as high K_2O contents (3.36–4.10 wt.%) and relatively high Mg# values (35.40 to 40.30) suggest the Tongcun intrusive complex was derived from partial melting of the thickened lower continental crust triggered by basaltic magma underplating plus additional input from the EM II mantle-derived basaltic melts. The Tongcun area was controlled by a compression setting related to the subduction of the Paleo–Pacific Plate in Mesozoic period.

© 2016 Elsevier B.V. All rights reserved.

1. Introduction

The close relationship between the adakites or adakitic rocks and porphyry Cu–Au deposits in arc settings (Thiéblemont et al., 1997), may indicate a genetic relationship between the slab–melting and Cu–Au mineralization. However, an increasing number of adakites and associated Cu–Au–Mo deposits were found in non–arc settings, e.g., the collisional orogenic zones or intracontinental tectonic settings, such as the Gangdese and Yulong copper deposit belts in Tibelt (Hou et al., 2011), the Dexing copper deposit in south China (Hou et al., 2013), and the Shakhtama porphyry Mo–Cu system in Eastern Transbaikalia, Russia (Berzina et al., 2014). Several hypotheses have been proposed for the origins of those adakites or adakitic rocks, e.g., partial melting of delaminated mafic lower crust (Wang et al., 2006), partial melting of thickened or normal lower crust with injection of mantle–derived mafic magmas (Hou et al., 2013; Ma et al., 2013; Berzina et al., 2014; Wang et al., 2015), partial melting of newly formed mafic lower crust (Atherton and Petford, 1993), crustal assimilation and fractional crystallization (AFC) processes from parental basaltic magmas (Richards and Kerrich, 2007). However, the genesis of those adakites or adakitic rocks as well as the associated deposits is still poorly understood. For example, so far two or more mechanisms above have been used to explain the generation of adakites in the Dexing deposit (Wang et al., 2006; Hou et al., 2011, 2013; Zhou et al., 2012). Meanwhile, compared

with the typical adakites as defined by Defant and Drummond (1990), even though the adakites referred above were derived from different sources or generated by different petrogenetic processes, their related magmatic-hydrothermal system can still generate the epithermal and porphyry deposits. Therefore, as confirmed by Wang et al. (2006), the genesis of adakites or adakitic rocks as well as their genetic relationship with porphyry Cu–Au–Mo mineralization needs to be further re-examined or clarified.

The history and characteristics of the intense tectono–magmatic activities during the Yanshanian (~200–80 Ma) in Southeast China have been deliberated in various studies (Jiang et al., 2011; Yang et al., 2012; S.H. Jiang et al., 2013; Li et al., 2013a, 2013b; Liu et al., 2013, 2014; Song et al., 2014; Li and Jiang, 2014). The geology of this region is characterized by the widespread occurrence of Mesozoic granitoids, which are associated with similarly widespread, economically important mineralization, e.g., W, Sn, U, Nb–Ta, Cu, Pb, Zn and Au (Mao et al., 2008, 2009, 2011a, 2011b, 2011c; J.W. Mao et al. 2013). These Mesozoic rocks and associated mineralization are different in their ages and mainly occur in three episodes, e.g., the first in the Late Triassic, the second in the Jurassic (Early Yanshanian), and the third in the Cretaceous (Late Yanshanian) (Mao et al., 2008, 2009, 2011a, 2011b, 2011c; J.W. Mao et al. 2013). As the most important metallogenic belt in SE China, The Qinzhou–Hangzhou metallogenic belt (QHMB) has been studied during recent years (Mao et al., 2011a, 2011b; Z.H. Mao et al., 2013; Zhou et al., 2015). Several large or super–large deposits (large deposit is defined as having no less than 500 thousand tons of Cu, Pb or Zn, 50 thousand tons of WO₃ and 20 tons of Au, and super–large deposits are at least five times larger upon the large deposits; Pei, 1995), most of which are associated with intrusive rocks, have been found in the eastern QHMB, including the famous Dexing porphyry Cu–Mo–Au, Jinshan Au and Yinshan Pb–Zn–Cu polymetallic deposits (Mao et al., 2011a, 2011b; Wang et al., 2011, 2012, 2013; Li et al., 2011, 2012; Guo et al., 2012), Xianglushan skarn W (Chen and Zhou, 2012), Dahutang porphyry W (Z.H. Mao et al., 2013), Yongping porphyry Cu–Mo (X.F. Li et al.,

2013), and Zhangshiba Pb–Zn deposits (Lu et al., 2005). Besides the Linghou Cu–Pb–Zn polymetallic deposit (Tang et al., 2015b), several promising occurrences have been found in east QHMB in Zhejiang province since 2008, such as Tongcun porphyry Mo–Cu (Qiu et al., 2013; Zeng et al., 2013), Yinshan Pb–Zn–Ag polymetallic (He et al., 2011), and Anji skarn–porphyry Fe–Pb–Zn polymetallic deposits (Xie et al., 2012).

The Tongcun Mo–Cu deposit is located in the northwest Zhejiang province, and is about 60 km away from the Dexing porphyry deposit (Fig. 1). The origins of the Tongcun intrusive rocks and porphyry Mo–Cu deposit have long been discussed (Wang, 2010; Qiu et al., 2011, 2013; Zeng et al., 2013; Zhang et al., 2013; Zhu et al., 2012; Zhu, 2014; Tang et al., 2015a). However, several problems still remained as follows:

1) The ore–forming metals of this deposit are not well constrained for lack of Pb isotopic data from the different intrusions and the main ore minerals, e.g. molybdenite and chalcopyrite.
2) The petrogenesis of the Tongcun intrusive complex is only reported in Chinese with the geochemistry, and whole-rock Sr–Nd–Pb isotopic data (only 3 lead isotopic data), and actually quite a few of the data are not of good quality due to the unusual loss on ignition value of more than 3% (Zhu, 2014). Moreover, the adakitic features of those intrusions have not been well understood, and the Dayutang intrusion has not been studied before.
3) The recognition of lithologies of the Tongcun intrusive complex are confusing (Qiu et al., 2011, 2013; Zeng et al., 2013; Zhang et al., 2013; Zhu et al., 2012; Zhu, 2014). Additionally, previous zircon U–Pb dating has offered a wide range in emplacement ages for those intrusive units, varying from ~155.6 Ma to ~170 Ma (Qiu et al., 2013; Zeng et al., 2013; Zhu et al., 2014; Zhu, 2014).

Therefore, in this paper, we present a detailed account of zircon U–Pb geochronology using LA–ICP–MS and SHRIMP, petrology and geochemistry of the Tongcun late Jurassic adakitic intrusive rocks, combined with the Pb isotopes of sulfides and ⁴⁰Ar–³⁹Ar age of
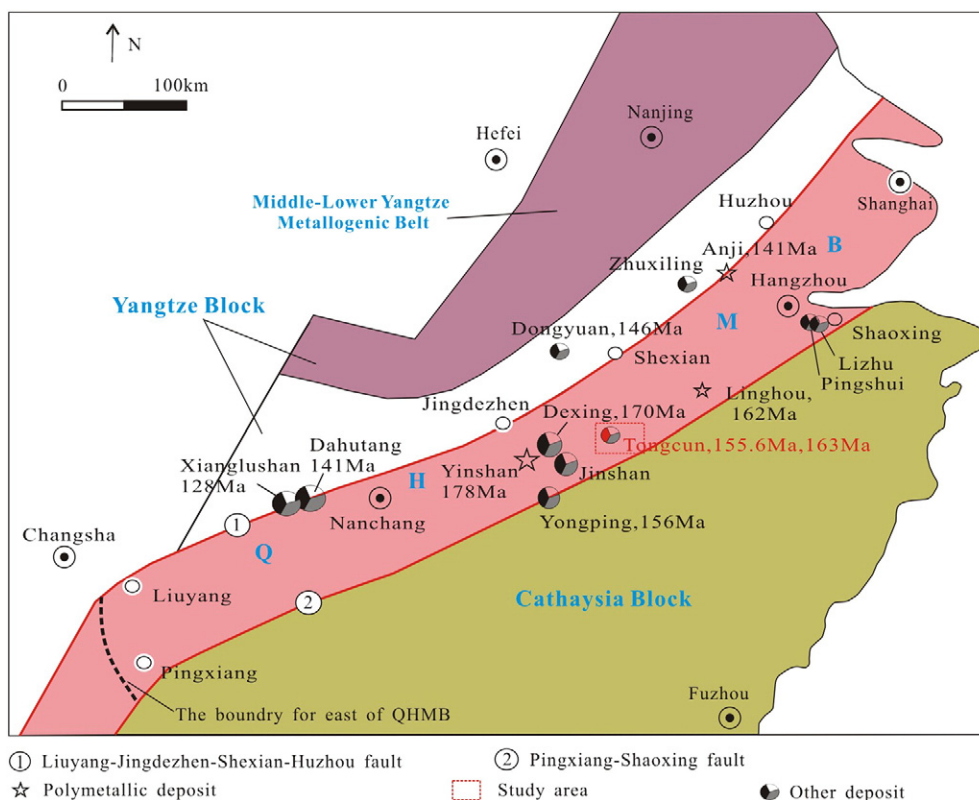

Fig. 1. Spatial–temporal distribution of Mesozoic ore deposits in the east of QHMB, Southeastern China. (Modified after Yang and Mei, 1997; Mao et al., 2011a; J.W. Mao et al., 2013.)

sericite associated with Cu mineralization, with aims to reveal the petrogenesis and tectonic significances of these adakitic intrusions, and provide new constraints on the genesis of the associated Mo–Cu mineralization.

2. Geological background

2.1. Regional geology

The QHMB, which connects the Yangtze and Cathaysian Blocks, extends from Qinzhou Bay of Guangxi Province to Hangzhou Bay of Zhejiang province, and is about 2000 km long and 100~150 km wide (Yang and Mei, 1997). The east QHMB is bounded by the Liuyang–Jingdezhen–Shexian–Huzhou fault in the north and the Pingxiang–Shaoxing fault in the south (Fig. 1). As a suture zone, the QHMB was interpreted to have resulted from the collision and extension between the Yangtze and Cathaysian Blocks, and two blocks were connected firstly during the Neoproterozoic period (about 825 Ma) (Hong et al., 2002; Shu, 2006; Yang et al., 2009). This period is characterized by volcanic arc igneous rocks (e.g., spilite– and quartz–keratophyre) in the basement rocks, which were termed as Shuanxiwu group in NW Zhejiang province, and coeval SEDEX Cu, Pb–Zn deposits, such as Pingshui and Luocheng copper deposits (Xu et al., 2015; Zhou et al., 2015). There is no evidence to support that the QHMB had reactivated during the Silurian and Triassic period (Mao et al., 2011a). Correspondingly, the clastic and carbonate rocks of neritic facies occurred in Devonian– middle Triassic Period, and the coal and few strata–bound polymetallic deposits of deep–water phases occurred along the ancient faults in Permian period (Yang and Mei, 1997; Li, 2000). And then, due to the conversion of tectonic regime from the Tethys to Paleo–Pacific, this belt had been reactivated several times during Yanshanian deformation (about from 135 Ma to 205 Ma) (Yang and Mei, 1997; Li, 2000; He et al., 2005; Mao et al., 2011a; He et al., 2015). Unfortunately, the accurate time when the Paleo–Pacific plates subducted beneath the Eurasian continent is still unclear. Dong et al. (2008) believed the time should be 165 Ma, whereas Mao et al. (2011c) constrained it to 175 Ma. Recently, Sun et al. (2015) confirmed that the Paleo-Pacific subduction occurred in 205 Ma. In summary, QHMB was controlled by compression associated with the subduction and collision from the paleo–Pacific plate (Yang et al., 2009; Mao et al., 2009; Li et al., 2013a). Furthermore, the east QHMB also experienced local extension events which were indicated by adakitic porphyries in Dexing deposit (Wang et al., 2006) and A-type granitoid complex in Lizhu and Nanling area (Hua et al., 2005; Jia et al., 2014). Till now, most of the Mesozoic tectono–magmatism events in the QHMB were related to the interaction between the Eurasian and Paleo–Pacific plates (Shu and Zhou, 2002; Wu et al., 2003; Zhou et al., 2006; Yang et al., 2009; Mao et al., 2009; Zheng et al., 2013; He et al., 2015). The formation mechanism and process for magmatism and mineralization are still debated, for example, 1) the tear-off and remelting of the subducted Izanagi Plate (170–160 Ma) and upwelling of asthenospheric magma and extensive mantle–crust interaction possibly induced by the plate window (160–150 Ma) (Mao et al., 2011a, 2011b; J.W. Mao et al., 2013); 2) lithosphere extension, thinning and underplating of mantle–derived magmas (Hua et al., 2005; Li et al., 2007a; Yang et al., 2009); 3) lithosphere extension and partial melting of delaminated lower crust (Wang et al., 2004). Those process were believed to give rise to intensive intracontinental tectonic–magmatic activities and metallogenesis in eastern China (Wang et al., 2004; Hua et al., 2005; Seton and Müller, 2008; Mao et al., 2009; J.W. Mao et al., 2013; Xiao et al., 2010; Zhang et al., 2013; He et al., 2015). Generally, the NNE and NE trending faults in eastern QHMB controlled the Yanshanian magmatic activities and the mineralization events (Yang and Mei, 1997; Yang et al., 2009). Most of the typical deposits in the QHMB (e.g., Dexing porphyry Cu and Yongpin porphyry-skarn Cu deposits) were formed in this period.

2.2. Deposit geology

The lithologic units in the Tongcun area are made up of Cambrian and Ordovician sedimentary rocks (Regional geological of Zhejiang Province, 1989), with nearly 90% of them being of the late Ordovician age (Fig. 2). The Upper Cambrian Xiyangshan Formation is only exposed in the southeast of Dayutang village, and has a thickness of about 40 m and consists mainly of argillaceous limestone and limestone. The Lower Ordovician sequences are composed of the Yinzhubu Formation and the Ningguo Formation. The former accounts for nearly 70% of all the rocks (Fig. 2), with a thickness of more than 600 m, and consists mainly of calcilutite and mudstone, and the latter has a thickness of 229 m, and consists mainly of shale and siliceous shale. The Middle Ordovician sequences are composed of the Hule Formation and the Yanwashan Formation. The former is 37 m in thickness and consists mainly of siliceous shale, and the latter has a thickness of 378 m, and consists mainly of argillaceous limestone and limestone. The Upper Ordovician Huangnigang Formation has a thickness of about 93 m and consists mainly of calcilutite and mudstone. These sedimentary sequences are all in conformable contact with the underlying and overlying rocks.

The prominent faults in the Tongcun deposit strike an NE-SW (F1), NS (F2) and NW-SE (F3, F4 and F5) (Fig. 2). F1 is a left lateral–thrust fault, dipping toward 100°–110° with a dip angle of 48°–55°. F5 is a normal fault dipping toward 60° with a dip angle of 47°. The attitudes and characteristics of the other faults have not been well documented. All the faults cut the NE striking syncline which was divided into three parts: 1) the SW part stretching from Longli to Dukengge village, striking 43° and plunging SW; 2) the middle part stretching from Dukengge to Xiangluling village, with the Upper Yinzhubu Formation occurring along the axis and the Middle or Lower Yinzhubu Formation along both limbs; and 3) the NE part stretching from Dayutang village to the Xishawu area.

The main intrusive rocks are composed by the Middle–Late Jurassic granitic complex, which is NE–SW striking and includes the Xiatongcun, Jiangjunwu, Huangbaikeng and Dayutang intrusions (Fig. 2). Due to intensive alteration, the lithologies of those intrusions are difficult to determine. The previous studies indicated that the former two and the latter two are mainly composed by monzogranite and granodiorite, respectively (Chen, 2011; Zhu et al., 2012; Jin et al., 2012). There are no clear boundaries to be found between different intrusive rocks. Previous zircon U–Pb dating data indicated that those intrusions were emplaced from ~155.6 Ma to ~170 Ma (Qiu et al., 2013; Zhu et al., 2014).

Widespread Mo–Cu mineralization is distributed in the Huangbaikeng, Jiangjunwu and Xiatongcun intrusive rocks, skarns and siltstone of the Ordovician Changwu Group. However, the economically viable ore bodies are mainly distributed around the latter two intrusions. Based on previous studies (Wang, 2010; Zeng et al., 2013; Jin et al., 2012), the Tongcun Mo–Cu deposit comprises two large orebodies (namely: No. I and No. II, Fig. 2) and seven smaller orebodies. These orebodies, have average thickness ranging from 4 to 25 m, along-strike length from 76 to 516 m, the dip length from 312 to 1065 m, and average grades of 0.069%–0.089% Mo. In addition to the Mo mineralization, Wang (2010) reported that there are two layers of Cu ores in No. I orebody and three layers of Cu ores in No. II orebody, with the total thickness of 9 and 8 m and the average grade of 0.47% and 0.27%, respectively. The early Mo (Cu) and late Cu mineralization events are characterized by the mineralogical assemblages of quartz + molybdenite + chalcopyrite and sericite + chalcopyrite + pyrite (Fig. 3), respectively. Wallrock alteration, ore mineralogy and mineral assemblages of this deposit have been given in Tang et al. (2015b).

3. Sample descriptions

The samples were collected mainly from the drill cores (numbered ZK408, ZK307, ZK004 and ZK007, respectively) of four intrusions in the Tongcun area. Their locations have been indicated in Fig. 2 and
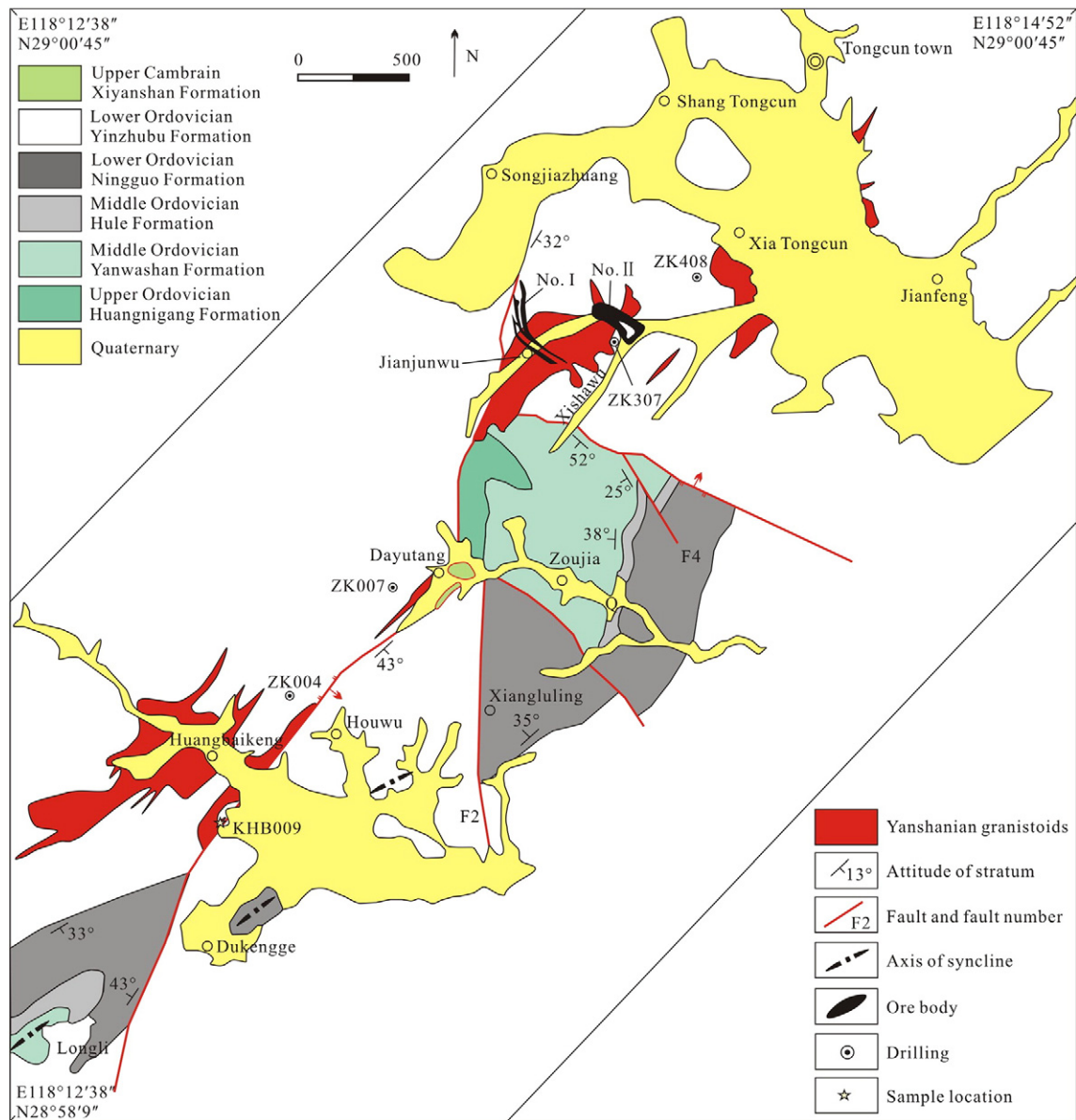
Fig. 2. Geological map of the Tongcun porphyry Mo–Cu deposit (Modified after the 2010 edition geologic map of Zhejiang No. 3 Geological Team).

described below. In summary, four samples were chosen for U–Pb dating, eight samples for geochemical analysis, five samples for Sr–Nd isotopes analysis, 14 samples (including the sulfides) for Pb isotope analysis and one sample for Ar–Ar dating. For lack of the suitable Cu ores, no sulfides from the late Cu mineralization were analyzed for Pb isotopic composition.

3.1. Monzogranite

Samples of KHB060–KHB61 (phase 1) were collected at 486 m and 499 m of ZK408 in the Xiatongcun village for geochemical analysis. KHB036 (phase 2) was collected at 160 m of ZK307 in the Jiangjunwu village for U–Pb dating. Those rocks show massive structure and fine–grained porphyritic–like texture (Fig. 4a), and are dominantly composed of plagioclase (~35 vol.%), quartz (20–25 vol.%), K–feldspar (~35 vol.%), biotite and hornblende (3–5 vol.%). The phenocrysts (~80 vol.%) show grain size ranging from 0.5 to 2.0 mm, whereas the matrix (~20 vol.%) has the general grain size of 0.1–0.2 mm.

3.2. Granodiorite

Samples of KHB065, KHB065–1 and KHB065–2 were collected at ~305 m of ZK004 from the Huangbaikeng village for geochemical analysis and U-Pb dating. KHB009 was collected from an outcrop in the Huangbaikeng village only for U–Pb dating. Additionally, five samples of KHB040–KHB44 were collected at 294 m, 335 m, 341 m, 354.2 m and 296 m of ZK007 in the Dayutang village, respectively. The former four were for geochemical analysis and the latter for U–Pb dating. The rocks of the Huangbaikeng and Dayutang intrusions also show massive structure and fine–grained porphyritic–like texture (Fig. 4c), and dominantly consist of plagioclase (40–45 vol.%), quartz (~20 vol.%), K–feldspar (~20 vol.%), biotite (~10 vol.%), and hornblende (<5 vol.%). The phenocrysts (75–80%) show grain size varying from 0.5 to 2.0 mm. The matrix (20–25 vol.%) has the grain size of 0.1–0.2 mm. Compared with the samples of KHB040–KHB44, KHB065, KHB065–1 and KHB065–2, the KHB009 is characterized by less phenocrysts (~35 vol.%) and more matrixes (~65 vol.%) (Fig. 4b).
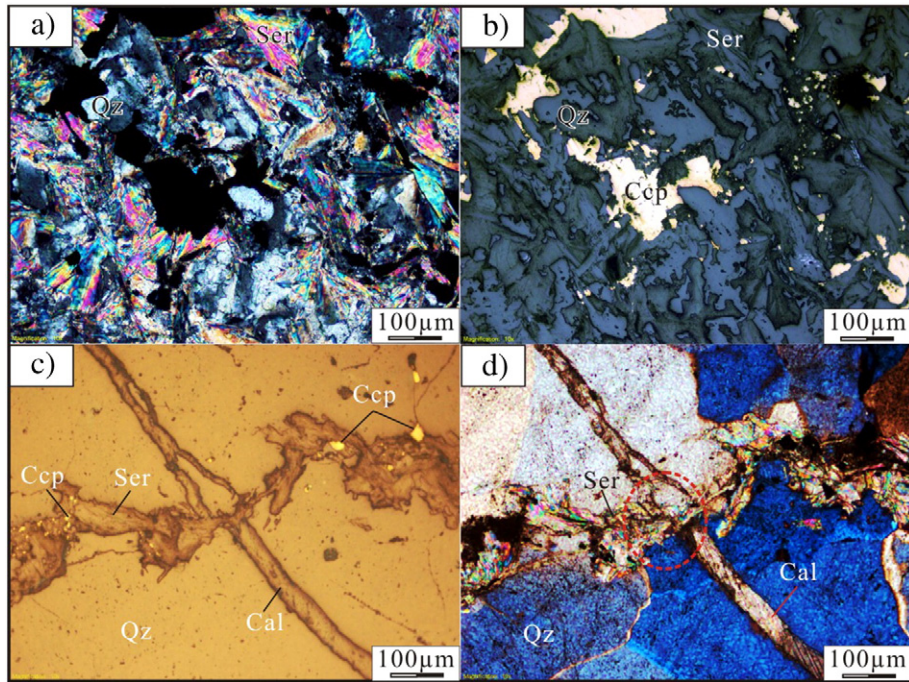
Fig. 3. Sericitization associated with the late Cu mineralization. (a) and (b) chalcopyrite (Ccp) coexists with sericite (Ser); (c) and (d) chalcopyrite coexists with sericite as a vein across the early quartz (Qz) + molybdenite (not showing in this picture) + chalcopyrite vein and calcite (Cal) vein.

4. Analytical methods

Fresh rock samples were divided in three groups: thin sections for petrography; 200 mesh powder for major, trace element, and Sr–Nd–Pb isotope analyses; 40–60 mesh crushing for selecting zircon grains.

4.1. Major and trace element analysis

Major and trace element compositions were analyzed in the Major and Trace Elements Laboratories of the Analytical Laboratory, Beijing Research Institute of Uranium Geology, China. For major element analyses, Philips AB-104L.PW2404 X–ray fluorescence spectroscopy (XRF) was used. The analytical uncertainties, based on the US Geological Survey rock standards BCR-1 and AVG-2, and the Chinese national rock standard GSR-3, are generally better than 1% for most of the oxides with the exception of TiO_2 (~1.5%) and P_2O_5 (~2.0%). Trace elements were analyzed using a Thermo Scientific Element XR inductively coupled plasma mass spectrometry (ICP-MS). The data quality was monitored by analyses of two US Geological Survey rock reference materials BCR-1 and BHVO-1. The analytical precision for most trace elements is better than 5%.

4.2. Sr-Nd-Pb isotopes analysis

Rb, Sr, Sm, Nd, and Pb isotopic analyses were performed on IsoProbe–T Thermal Ionization Mass Spectrometer (TIMS) at the Analytical Laboratory, Beijing Research Institute of Uranium Geology, China. Procedural blanks are <50 pg for Sm and Nd, 2×10^{-10} pg for Rb and Sr, and <100 pg for Pb. The isotopic ratios were corrected for mass fractionation by normalizing to $^{86}Sr/^{88}Sr = 0.1194$ and $^{146}Nd/^{144}Nd = 0.7219$, respectively. The measured values for the JMC Nd standard and NBS987 Sr standard were $^{143}Nd/^{144}Nd = 0.512109 \pm 3$ (2σ) and $^{87}Sr/^{86}Sr = 0.710250 \pm 7$ (2σ), respectively. Repeated analyses of Pb isotope standard NBS981 yielded $^{208}Pb/^{206}Pb = 2.164940 \pm 15$, $^{207}Pb/^{206}Pb = 0.914338 \pm 7$ and $^{204}Pb/^{206}Pb = 0.0591107 \pm 2$. The detailed analytical procedures were described in Chen et al. (2000).

4.3. Cathodoluminescence (CL) images of zircon

In order to identify zircon internal textures and select target spots for U–Pb dating, the SEM cathodoluminescence (CL) images of zircons from KHB044, KHB065–1 and KHB009 were photographed by using a JSM–6510 electron microprobe coupled with a Gatan CL Detector at Beijing
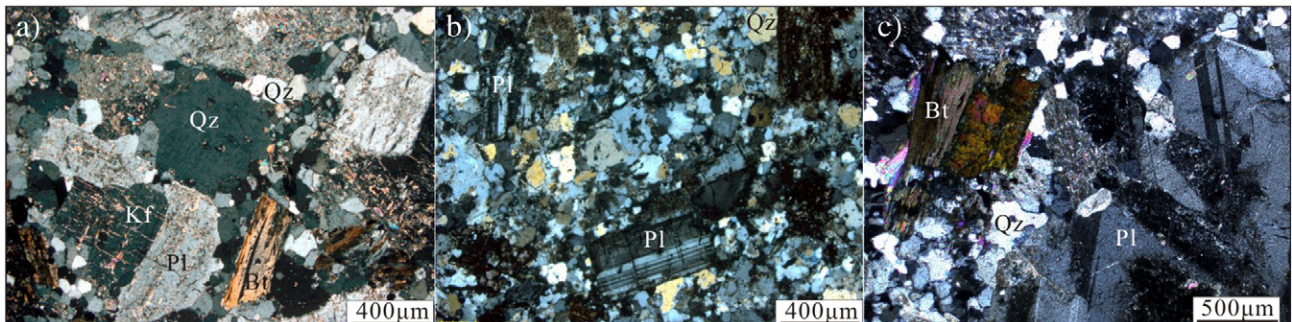
Fig. 4. Micrographs of monzogranite (phase 1) and granodiorites in the Tongcun ore deposit. (a) Fine–grained monzogranite; (b–c) Porphyritic-like texture of fine–grained granodiorite.

Geoanalysis Co., Ltd., and zircons from KHB036 were conducted by using a HITACHI S3000–N Scanning Electron Microscope (SEM) equipped with GATAN Chroma CL probe at the Beijing SHRIMP Centre, Institute of Geology, Chinese Academy of Geological Sciences, Beijing, China.

4.4. LA–ICP–MS zircon U–Pb dating

In–situ zircon U–Pb dating were performed on an Agilent 7500cs quadrupole ICPMS with a 193 nm Coherent Ar–F gas laser and the Resonetics S155 ablation cell at the University of Tasmania in Hobart. The downhole fractionation, instrument drift and mass bias correction factors for Pb/U ratios on zircons were calculated using 2 analyses on the primary (91500 standard of Wiedenbeck et al., 1995) and 1 analysis on each of the secondary standard zircons (Temora or GJ–1, Black et al., 2004; Jackson et al., 2004) analyzed at the beginning of the session and every 15 unknown zircons (roughly every half an hour) using the same spot size and conditions as used on the samples. The correction factor for the $^{207}Pb/^{206}Pb$ ratio was calculated using large spots of NIST610 analyzed every 30 unknowns and corrected using the values recommended by Baker et al. (2004). Each analysis on the zircons began with a 30-second blank gas measurement followed by a further 30 s of analysis time when the laser was switched on. Zircons were sampled on 32 μm spots using the laser at 5 Hz and a density of approximately 2 J/cm². A flow of He carrier gas at a rate of 0.35 L/min carried particles ablated by the laser out of the chamber to be mixed with Ar gas and carried to the plasma torch. Isotopes measured were ^{49}Ti, ^{56}Fe, ^{90}Zr, ^{178}Hf, ^{202}Hg, ^{204}Pb, ^{206}Pb, ^{207}Pb, ^{208}Pb, ^{232}Th and ^{238}U with each element being measured every 0.16 s with longer counting time on the Pb isotopes compared to the other elements. The data reduction used was based on the method outlined in detail in Black et al. (2004), Meffre et al. (2008), Paton et al. (2010) and Sack et al. (2011).

4.5. SHRIMP zircon U–Pb dating

The SHRIMP zircon U–Pb analyses were performed on the SHRIMP II at the Beijing SHRIMP Centre, Institute of Geology, Chinese Academy of Geological Sciences, Beijing, China. The analysis procedures were described in detail by Compston et al. (1992), Williams (1998) and Song et al. (2002). Elemental abundances of U, Th and Pb were calibrated by analyses of M257 reference zircon, with U concentration of 840 ppm (Nasdala et al., 2008). The $^{206}Pb/^{238}U$ age was calibrated using the standard zircon of TEMORA 1 with age of 416.8 ± 0.3 Ma. Mass resolution is over 5000 (1% peak height). A primary O_2^- ion beam of 4–5 nA and 10 kV, focused to a 20–25 μm spot diameter on the target were used. A TEMORA 1 analysis was undertaken after every 3–4 analyses of the unknowns. The common Pb correction was based on the measured ^{204}Pb (Composton et al., 1984). Uncertainties given for individual analyses (ratios and ages) are at 1σ level whereas the uncertainties in calculated weighted mean ages are reported as the 95% confidence level. Concordia plots and weighted mean age calculations were carried out using ISOPLOT/Ex 3.23 (Ludwig, 2003).

4.6. Sericite Ar–Ar dating method

Sericite of KHB039, which formed during the sericite + chalcopyrite + pyrite stage, mainly selected from a sericite–chalcopyrite vein (Fig. 3) in the granodiorite at the ZK307 drilling (at 184–215 m underground) in the Jiangjunwu orefield. Most of them occur as euhedral aggregates with a diameter of about 1 to 2 mm. Sericite separates were carefully handpicked under a binocular microscope, with purity over 99%. The sample separates, together with the monitoring standard samples were irradiated within a quartz vial in anuclear reactor at the Chinese Institute of Atomic Energy, Beijing. Step–heating $^{40}Ar/^{39}Ar$ analyses were performed on noble gas mass spectrometry Helix SFT at the Analytical Laboratory, Beijing Research Institute of Uranium

Geology, China. Procedural blanks are $<1 \times 10^{-15}$ mol at room temperature and $<1 \times 10^{-14}$ mol for ^{40}Ar. The monitor used in this work is the internal Fangshan biotite (ZBH–25) standard with an age of 132.7 ± 1.2 Ma and amphibole (GBW04418) standard with an age of 2060 ± 8 Ma, which were also irradiated. The decay constant for ^{40}K used in the calculation is 5.543×10^{-10} year^{-1} (Steiger and Jäger, 1977).

5. Results

5.1. Geochronology

5.1.1. Zircon LA–ICP–MS U–Pb dating

Zircon U–Pb isotope data for the granitic samples from the Tongcun complex are presented in Table 1. The zircon grains are euhedral, and their elongation ratios are mostly between 2:1 and 4:1. Most of them are transparent and colorless under the optical microscope. Oscillatory zonings of typical magmatic zircons are common and some inherited cores can also be observed under CL images. Zircons from those granodiorites have consistent U and Th contents with Th/U ratios of 0.12–0.24, 0.16–0.62 and 0.10–0.71, respectively (Table 1). Those characteristics show that all zircon grains are magmatic origin.

A total of 48 zircon spots were analyzed, of which 29 yield a concordant age. Zircon U–Pb concordia diagrams for the Dayutang granodiorite (KHB044) and the Huangbaikeng granodiorite (KHB065 and KHB009) are shown in Fig. 5. The measured $^{206}Pb/^{238}U$ ratios give a weighted mean age of 160.1 ± 1.5 Ma (MSWD = 1.6, n = 11) for KHB044 (Fig. 5a), 159.2 ± 1.2 Ma (MSWD = 0.46, n = 9) for KHB065 (Fig. 5b), and 158.6 ± 4.1 Ma (MSWD = 2.4, n = 5) for KHB009 (Fig. 5c).

5.1.2. Zircon SHRIMP U–Pb dating

Zircons of Jiangjunwu monzogranite (KHB036) are 100–300 μm long, mostly euhedral, prismatic and colorless with oscillatory zoning (Fig. 6), which are all features indicative of a magmatic origin. Most of them have inherited cores, which show different optical characteristics with the edges in cathodoluminescence images (Fig. 6). Nonetheless, both the overgrowths and the inherited cores of the zircons have consistent U and Th contents, and show Th/U ratios of 0.17–0.27 and 0.60–0.1.36, respectively. The results of SHRIMP U–Pb zircon dating are summarized and illustrated in Table 2 and Fig. 6, respectively. These analyses of magmatic zircons yield concordant results with weighted mean $^{206}Pb/^{238}U$ ages of 148.1 ± 1.7 Ma (n = 14). Seven inherited cores give the age of 820 ± 14 Ma, 789 ± 14 Ma, 879 ± 16 Ma, 783 ± 15 Ma, 796 ± 12 Ma, 753 ± 14 Ma and 749 ± 11 Ma, respectively. All of them yield concordant results with weighted mean $^{206}Pb/^{238}U$ ages of 780 ± 29 Ma (n = 6).

5.1.3. Ar–Ar age of sericite

The Ar–Ar isotopic data of sericite (KHB039) are given in Table 3 and illustrated in Fig. 7. The results yield a well–defined plateau age of 155.55 ± 0.88 Ma (Fig. 7a), and a normal and inverse isochron age of 155.50 ± 0.9 Ma and 155.53 ± 0.9 Ma, respectively (Fig. 7b and c). The initial $^{40}Ar/^{36}Ar$ values were 300.4 ± 15.5 and 300.2 ± 15.3 Ma, respectively.

5.2. Major and trace elements geochemistry

Major and trace element analyses are presented in Table 4. The Dayutang granodiorite, Huangbaikeng granodiorite and Xiatongcun monzogranite have homogeneous major element compositions with high SiO_2 of 67.41–70.7 wt.%, Al_2O_3 of 14.82–15.94 wt.%, and $K_2O + Na_2O$ of 7.47–7.79 wt.%, and low MnO (0.02–0.05 wt.%), $Fe_2O_3^T$ (2.33–2.78 wt.%), MgO (0.73–0.90 wt.%), P_2O_5 (0.10–0.13 wt.%) and TiO_2 (0.31–0.37 wt.%). They also have homogeneous Mg# varying from 35.40 to 40.30 (Table 4). All of the samples fall into the

Table 1
Zircon LA–ICP–MS U–Pb data for the Tongcun granitoids.

Spots	U	Th	Th/U	$^{206}Pb/^{238}U$		$^{208}Pb/^{232}U$		$^{207}Pb/^{206}Pb$		$^{206}Pb/^{238}U$		^{207}Pb cor $^{206}Pb/^{238}U$		$^{208}Pb/^{232}Th$		$^{208}Pb/^{206}Pb$	
	ppm			Ratio	±1σ(%)	Ratio	±1σ (%)	Ratio	±1σ(%)	Age	±1σ	Age	±1σ	Age	±1σ	Age	±1σ
KHB044 Dayutang granodiorite																	
OC11B468	833	187	0.22	0.0249	1.0	0.0093	2.0	0.0541	1.8	159	2	158	2	187	4	375	42
OC11B471	589	100	0.17	0.0248	1.1	0.0075	3.1	0.0498	2.2	158	2	158	2	151	5	186	52
OC11B466	572	88	0.15	0.0248	1.1	0.0079	2.7	0.0510	2.5	158	2	158	2	158	4	241	58
OC11B474	697	144	0.21	0.0248	1.7	0.0079	4.5	0.0478	4.1	158	3	158	3	159	7	91	96
OC11B470	603	133	0.22	0.0250	1.1	0.0076	2.6	0.0501	2.3	159	2	159	2	153	4	199	53
OC11B473	689	91	0.13	0.0250	1.0	0.0079	2.7	0.0480	2.3	159	2	159	2	159	4	100	55
OC11B472	907	217	0.24	0.0250	1.0	0.0079	1.9	0.0490	1.9	159	2	159	2	158	3	148	45
OC11B465	831	169	0.20	0.0254	1.0	0.0083	2.1	0.0491	2.2	161	2	161	2	167	4	151	52
OC11B463	684	137	0.20	0.0256	1.1	0.0083	2.4	0.0507	2.0	163	2	163	2	168	4	229	46
OC11B467	619	126	0.20	0.0256	1.0	0.0088	2.5	0.0512	2.3	163	2	163	2	177	4	251	53
OC11B464	573	69	0.12	0.0257	1.1	0.0080	2.9	0.0500	2.3	164	2	164	2	160	5	196	53
KHB065–1 Huangbaikeng granodiorite																	
OC11B490	493	92	0.19	0.0247	1.2	0.0077	2.8	0.0489	2.9	157	2	157	2	154	4	144	67
OC11B483	400	140	0.35	0.0249	1.2	0.0079	2.2	0.0511	2.7	159	2	158	2	159	4	247	61
OC11B485	552	106	0.19	0.0249	1.1	0.0082	2.6	0.0496	2.3	158	2	158	2	165	4	175	54
OC11B484	331	204	0.62	0.0249	1.3	0.0080	1.9	0.0496	3.2	159	2	158	2	161	3	178	75
OC11B486	808	168	0.21	0.0250	1.1	0.0086	2.0	0.0520	1.9	159	2	159	2	174	4	284	42
OC11B477	813	189	0.23	0.0251	1.0	0.0082	2.2	0.0513	2.6	160	2	159	2	164	4	255	60
OC11B487	459	84	0.18	0.0252	1.3	0.0084	2.6	0.0505	2.6	161	2	160	2	170	4	217	60
OC11B491	588	113	0.19	0.0253	1.0	0.0078	2.4	0.0510	2.3	161	2	160	2	157	4	242	54
OC11B478	444	69	0.16	0.0253	1.2	0.0081	3.0	0.0505	2.8	161	2	161	2	162	5	217	64
KHB009–1 Huangbaikeng granodiorite																	
NO07A095	675	62	0.10	0.0246	1.0	0.0075	3.2	0.0501	1.9	157	2	156	2	151	5	201	45
OC11B383	373	75	0.20	0.0250	1.3	0.0114	2.7	0.0620	2.9	159	2	157	2	230	6	675	61
OC11B388	68	46	0.67	0.0249	2.5	0.0087	4.0	0.0577	6.3	158	4	157	4	176	7	517	139
OC11B380	470	150	0.32	0.0253	1.7	0.0079	2.7	0.0514	3.6	161	3	160	3	159	4	258	84
OC11B382	822	261	0.32	0.0257	1.2	0.0080	2.7	0.0518	3.1	164	2	163	2	161	4	276	70
OC11B389	1652	828	0.50	0.0262	0.9	0.0085	1.4	0.0513	1.4	167	1	167	1	170	2	255	33
OC11B377	1914	1356	0.71	0.0266	0.9	0.0083	1.3	0.0506	1.3	169	1	169	1	166	2	222	29
OC11B386	1891	293	0.15	0.0269	0.9	0.0087	1.7	0.0518	1.3	171	2	170	2	175	3	275	29
OC11B387	1427	417	0.29	0.0281	0.9	0.0100	1.7	0.0525	1.5	179	2	178	2	200	3	305	33

granodiorite to granite fields in the TAS classification diagram (Fig. 8a) and belong to the high–K calc–alkaline series in the K_2O versus SiO_2 diagram (Fig. 8b). They are characterized by metaluminous to peraluminous compositions with A/CNK near to 1.0 (ranging from 0.97 to 1.05) and A/NK ranging from 1.41 to 1.51 (Fig. 8c).

These intrusions have total REE ($\sum$ REE) and HREE ($\sum$ HREE) contents of 121.94–150.95 ppm and 12.25–15.80 ppm, respectively. They also show strong fractionation between the light REE and heavy REE (LREE/HREE = 6.65–8.11 and La_N/Yb_N = 28–41) with weakly negative Eu anomalies (δEu = 0.70–0.79) (Fig. 9a). They have high Sr (481–584 ppm), low Y (6.11–8.68 ppm) and Yb (0.59–0.77 ppm) contents with Sr/Y ratios of 56–80 and La_N/Yb_N ratios of 28.08–40.98.

They show relative enrichment in large ion lithophile elements (LILEs) such as Rb, Th, U and Pb, and remarkable depletion in high field strength elements (HFSEs) of Nb, Ta, P, Zr and Ti (Fig. 9b).

5.3. Sr–Nd–Pb isotopes

The initial $^{87}Sr/^{86}Sr$ (I_{Sr}) ratios and $\varepsilon_{Nd}(t)$ values of five rock samples have been calculated corresponding to the zircon U–Pb ages (~160 Ma). Sr, Nd and Pb isotopic compositions of the Dayutang, Huangbaikeng granodiorites and the Xiatongcun monzogranite are presented in Tables 5 and 6, and shown in Figs. 10a and 11. They have uniform I_{Sr} values of 0.7083–0.7092, $\varepsilon_{Nd}(t)$ of − 6.3 to − 7.3 and T_{2DM} values of 1.46–1.54 Ga. Eight rock samples have similar Pb isotopic compositions of ($^{206}Pb/^{204}Pb)_i$ = 18.114–18.263, ($^{207}Pb/^{204}Pb)_i$ = 15.596–15.621, ($^{208}Pb/^{204}Pb)_i$ = 38.306–38.423). Six sulfides from Tongcun Mo—Cu deposit have Pb isotopic compositions of $^{206}Pb/^{204}Pb$ = 18.314–18.427, $^{207}Pb/^{204}Pb$ = 15.589–15.651, $^{208}Pb/^{204}Pb$ = 38.374–38.650, which are similar to those of eight rock samples from Tongcun intrusive complex.

6. Discussions

6.1. Timing of magma emplacement

Previous studies suggested that the Tongcun complex is composed by the Huangbaikeng, Jiangjunwu and Xiatongcun intrusions with a wide formation ages varying from ~155.6 Ma to ~170 Ma (Qiu et al., 2013; Zeng et al., 2013; Zhu et al., 2014; Zhu, 2014). The new LA–ICP–MS zircon ages of 160.1 ± 1.5 Ma for Dayutang granodiorite and two groups of 159.2 ± 1.2 and 158.6 ± 4.1 Ma for Huangbaikeng granodiorite are more consistent with each other as well as the associated mineralization ages, e.g., the molybdenite Re-Os age of 162 Ma (Zhang et al., 2013) and the sericite Ar-Ar age of 155.53 ± 0.90 Ma (this paper) within error limits. Therefore, three new ages are credible and this complex should include the Dayutang intrusion. As the new SHRIMP zircon age of 148.1 ± 1.7 Ma for the Jiangjunwu monzogranite, two explanations can be given:

1) It is a coeval magmatic event with the other rock units in this complex. Based on the previous studies from Qiu et al. (2013), this monzogranite (granite porphyry) formed in 159.9 Ma. The difference (~12 Ma) from two dating methods may result from the uncertainty (±4%, 2RSD) of LA–ICP–MS as X.H. Li et al. (2015) reported.

2) There were two stages of monzogranite in the Jiangjunwu intrusion, the first stage (phase 1) formed in 159.9 Ma (Qiu et al., 2013). The late monzogranite (phase 2) formed in 148.1 ± 1.7 Ma, which is supported by considerable inherited cores in zircons, comparing with the early monzogranite and other intrusive rocks in our and the previous studies. Additionally, the ages of these inherited cores were consistent with those in other intrusive rocks (Table 7, Fig. 6b). Moreover, the late Jurassic magmatic
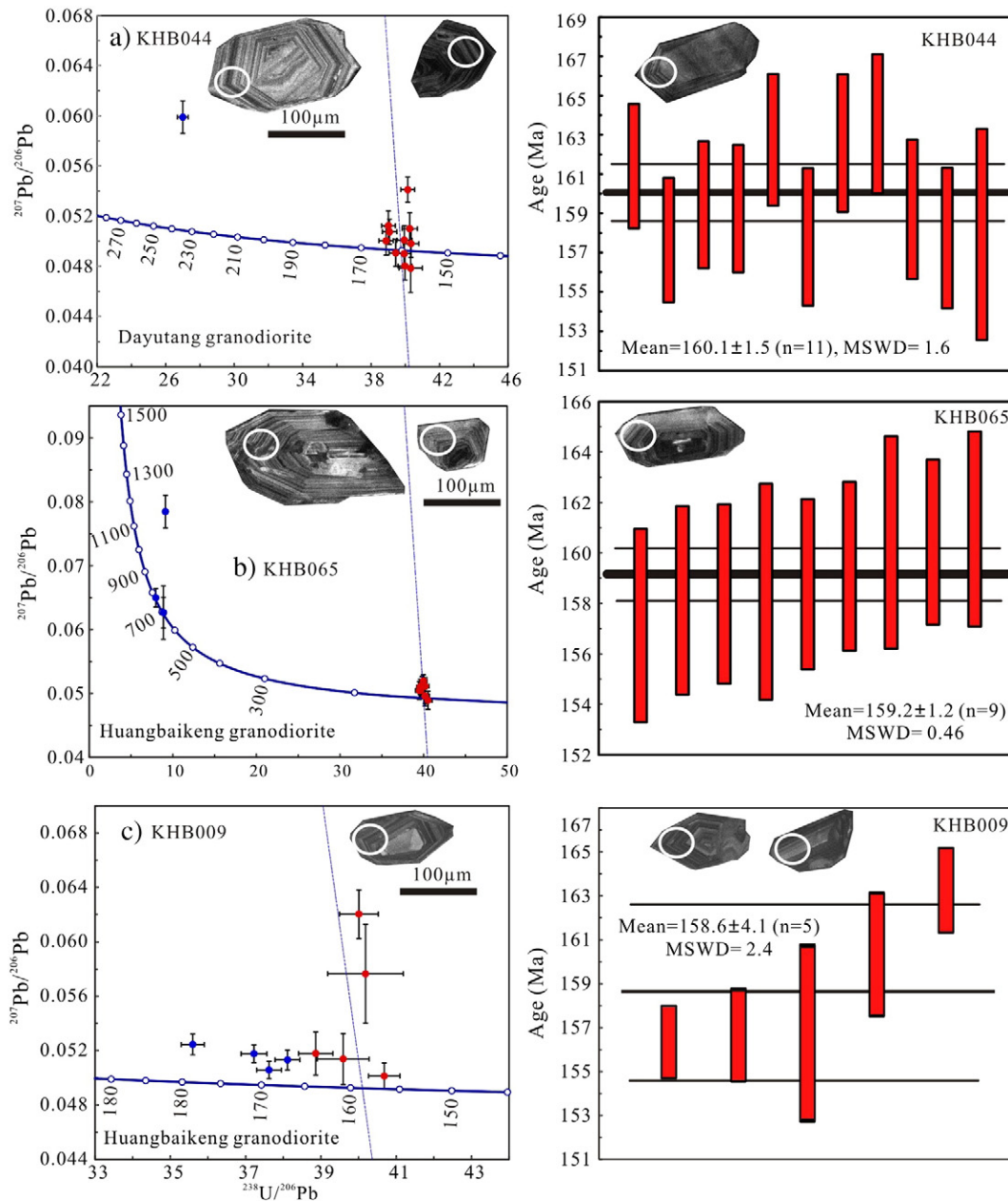
Fig. 5. Concordia diagram showing $^{238}U/^{206}Pb$ vs. $^{207}Pb/^{206}Pb$ results and the weighted average $^{206}Pb/^{238}U$ age for single–grain zircon of granitoids from the Tongcun intrusive complex (Analyses in red color used in age calculation mainly).

event has been reported in several other deposit in NW Zhejiang province, such as the Wushanguan complex (139.2–150.2 Ma) in the Anji polymetallic deposit (Xie et al., 2012; Rehandling with the 91500 zircon standard), the Shanxi-Guanshan complex (147.2–150.1 Ma) in the Lizhu Fe-Zn-Mo skarn deposit (Gu et al., 2011), Mugua, Jiemeng and Datongkeng intrusions in Chun'an area (142.2–148.6 Ma) (Li et al., 2013a, 2013b).

Therefore, the second interpretation should be more acceptable and it indicates that the Tongcun intrusive complex formed mainly in late Jurassic period from 160 Ma to 148 Ma.

6.2. Sericite Ar-Ar dating for late Cu mineralization

Molybdenite Re–Os dating by Zhang et al. (2013), Zeng et al. (2013) and Tang et al. (2015a) demonstrated that the early Mo

(Cu) mineralization in the Tongcun deposit occurred at 162.2–163.9 Ma. New geological evidence confirmed that there is a late Cu mineralization event occurred slight later than Mo (Cu) mineralization in this deposit (Tang et al., 2015a). As the typical Cu–bearing sulfide of Cu mineralization in the Tongcun deposit, chalcopyrite is typically intergrown with sericites (Fig. 3) in monzogranite (phase 1). The $^{40}Ar–^{39}Ar$ dating of those sericite shows excellent agreement among the plateau age, isochron age and inverse isochron age, within the applicable analytical uncertainty (Table 3, Fig. 7). Moreover, the isochron and inverse isochron treatments of the data indicate that initial $^{40}Ar/^{36}Ar$ ratios are well consistent with atmospheric value of 298.56 ± 0.31 Ma (Lee et al., 2006) within error uncertainty, suggesting the absence of excess argon. Therefore, the plateau age of 155.53 ± 0.90 Ma is believed as a better estimate of the crystallization age of the sericite, and also represents the age of the late Cu mineralization event in the Tongcun deposit.
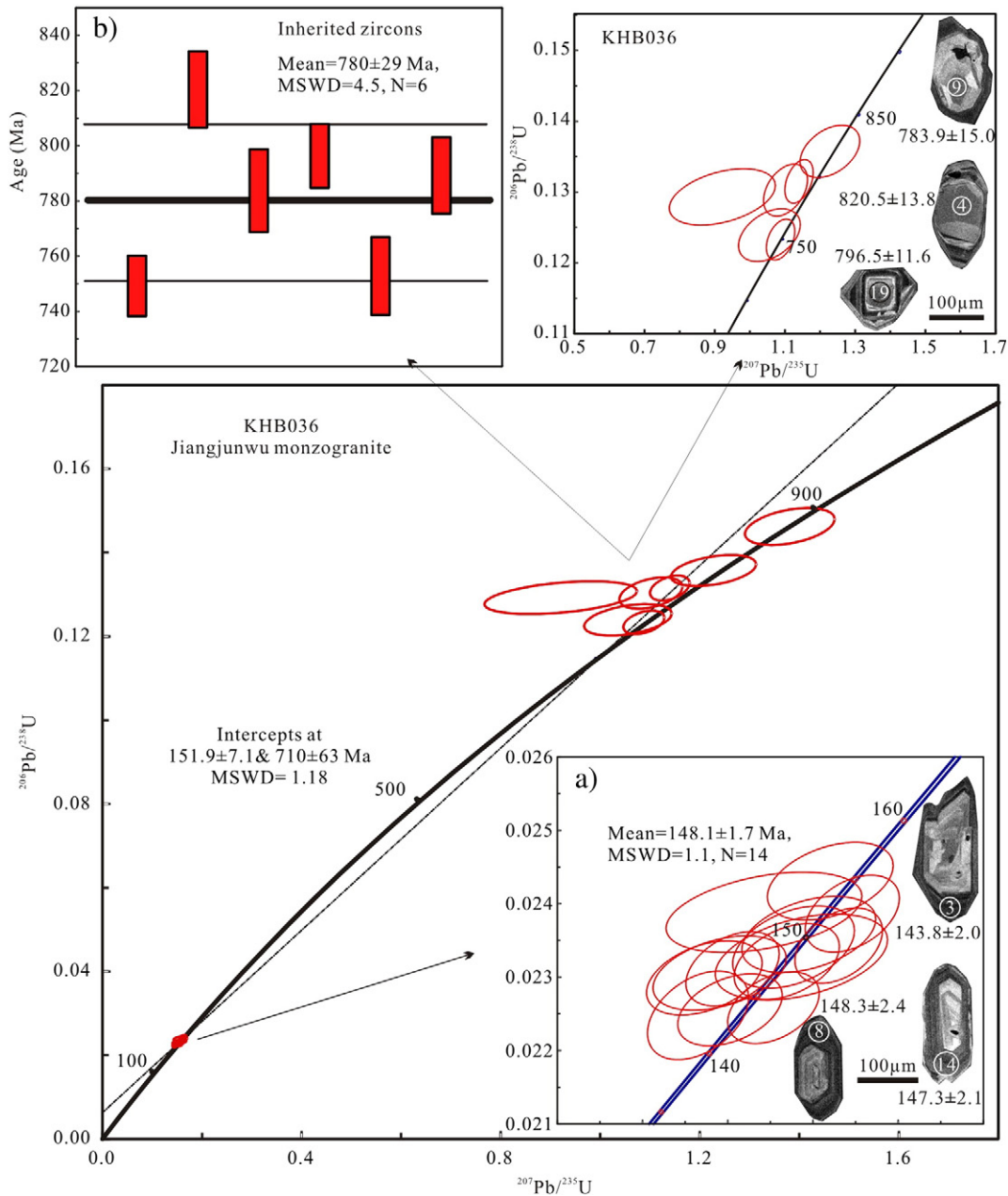
Fig. 6. SHRIMP Zircon U–Pb weighted mean ages and concordia diagrams of the Jiangjunwu monzogranite (phase 1).

6.3. Petrogenesis of the Tongcun granitoids

6.3.1. Petrogenetic type and adakitic affinities of the Tongcun granitoids

The Dayutang, Huangbaikeng granodiorites and the Xiatongcun monzogranite (phase 1) show the chemical compositions of Na_2O more than 3.2%, the aluminum saturation index (ASI) A/CNK less than 1.1. Those characteristics are consistent with I–type granites and different from S–type granites (Chappell and White, 2001). Those granitoids have the medium differentiation indexes (DI) of 77.51– 81.36, which are less than the typical highly fractionated I–type granite in China, e.g., the Fogang granites (82–94) (Li et al., 2007b) and Chayu granite (82–92) (Zhu et al., 2009), indicating that those intrusions are not highly fractionated. Therefore, as concerned by F.Y. Wu et al. (2007), the aluminum saturation index was reliable in this discrimination. Different with A–type granite (Whalen et al., 1987), all the Tongcun granitoids are relatively low in $Zr + Nb + Y + Ce$ (<180 ppm), FeO^T/MgO and $(K_2O + Na_2O)/CaO$, falling into the unfractionated granite field (Fig.

11c and d). Combined with SiO_2 of 67.41–70.7 wt.% and high K_2O of 3.36–4.10 wt.% (Table 4), we classify them as the typical high–K calc–alkaline I–type granitoids.

Moreover, compared with the typical adakites of Defant and Drummond (1990), the Tongcun granitoids have most of the adakitic geological signatures, e.g., high SiO_2 (≥56%) and Al_2O_3 (≥15%), low MgO (<3%), low Y and heavy REE concentrations (Y < 20 ppm, Yb < 2 ppm), high Sr (>400 ppm) and low high–field strength elements (HFSEs). In Sr/Y vs. Y and $(La/Yb)_N$ vs. Yb_N diagrams, all the samples plot in the adakite fields (Fig. 12a and b).

Therefore, the Tongcun complex can be classified as high–K calc–alkaline I–type and adatikitic granitoids.

6.3.2. Magma source of the Tongcun granitoids

The geological characteristics of the Tongcun intrusive rocks indicate the mantle–derived component was involved in the parent magma. Firstly, in $\varepsilon_{Nd}(t)$ vs. I_{Sr} diagram, the Tongcun granitoid samples plot

Table 2
Zircon SHRIMP U–Pb data for the Jiangjunwu monzogranite (KHB036, phase 2).

Spot	$^{206}Pb_c$(%)	U ppm	Th	$^{206}Pb*$	$^{232}Th/^{238}U$	$^{207}Pb*/^{206}Pb*$	±%	$^{207}Pb*/^{235}U$	±%	$^{206}Pb*/^{238}U$	±%	$^{206}Pb/^{238}U$ (Ma)	$^{207}Pb/^{206}Pb$ (Ma)	$^{207}Pb/^{206}Pb$ (Ma)
KHB036–1.1	–	1059	174	21.7	0.17	0.05003	1.7	0.1646	2.2	0.02386	1.4	152.0 ± 2.2	196 ± 39	143 ± 4
KHB036–2.1	0.37	1618	308	33.9	0.20	0.0483	2.6	0.1621	3.0	0.02431	1.4	154.8 ± 2.2	116 ± 62	183 ± 8
KHB036–3.1	0.11	1674	364	32.5	0.22	0.0483	2.3	0.1503	2.7	0.02255	1.4	143.8 ± 2.0	115 ± 54	137 ± 5
KHB036–4.1	0.26	105	70	12.2	0.69	0.0656	4.2	1.228	4.6	0.1357	1.8	820 ± 14	795 ± 88	766 ± 30
KHB036–5.1	0.39	275	159	30.9	0.60	0.0613	3.3	1.102	3.8	0.1303	1.9	789 ± 14	651 ± 70	721 ± 26
KHB036–6.1	0.28	81	54	10.2	0.69	0.0685	3.9	1.381	4.3	0.1462	2.0	879 ± 16	885 ± 80	830 ± 34
KHB036–7.1	0.14	1299	216	26.2	0.17	0.0489	2.5	0.1577	3.0	0.02341	1.6	149.2 ± 2.3	141 ± 60	143 ± 7
KHB036–8.1	0.06	898	88	18.0	0.10	0.0494	3.9	0.1586	4.2	0.02327	1.7	148.3 ± 2.4	169 ± 90	148 ± 15
KHB036–9.1	1.77	71	93	7.98	1.36	0.0517	11	0.921	11	0.1292	2.0	783 ± 15	272 ± 243	718 ± 31
KHB036–10.1	–	1771	286	35.6	0.17	0.05047	1.5	0.1630	2.1	0.02343	1.4	149.3 ± 2.1	217 ± 35	163 ± 4
KHB036–11.1	0.25	999	111	20.0	0.12	0.0490	2.1	0.1569	2.6	0.02321	1.5	147.9 ± 2.1	150 ± 50	135 ± 5
KHB036–12.1	0.03	1324	153	26.8	0.12	0.0491	2.9	0.1595	3.3	0.02358	1.5	150.3 ± 2.2	151 ± 68	151 ± 13
KHB036–13.1	0.16	1334	232	26.5	0.18	0.04725	1.9	0.1506	2.4	0.02311	1.4	147.3 ± 2.1	62 ± 46	138 ± 6
KHB036–14.1	0.64	769	100	15.9	0.13	0.0468	4.7	0.1543	4.9	0.02389	1.5	152.2 ± 2.3	41 ± 112	131 ± 18
KHB036–15.1	–	1745	457	33.8	0.27	0.04990	1.8	0.1554	2.3	0.02258	1.4	144.0 ± 2.0	190 ± 41	145 ± 3
KHB036–16.1	0.19	1902	453	36.8	0.25	0.04727	2.0	0.1465	2.7	0.02248	1.8	143.3 ± 2.5	63 ± 48	131 ± 6
KHB036–17.1	0.18	1321	193	26.1	0.15	0.0465	2.7	0.1473	3.0	0.02299	1.4	146.5 ± 2.1	21 ± 64	139 ± 8
KHB036–18.1	0.31	1297	229	25.8	0.18	0.0469	3.1	0.1491	3.5	0.02306	1.5	146.9 ± 2.1	44 ± 75	126 ± 9
KHB036–19.1	0.21	339	219	38.4	0.67	0.0629	1.7	1.140	2.3	0.1315	1.5	796 ± 12	704 ± 31	745 ± 16
KHB036–20.1	0.79	88	96	9.46	1.13	0.0618	5.1	1.056	5.5	0.1239	2.0	753 ± 14	667 ± 110	688 ± 24
KHB036–21.1	0.11	253	175	26.9	0.71	0.0640	1.9	1.088	2.5	0.1233	1.5	749 ± 11	741 ± 40	72 1 ± 15

1) Errors are 1σ, Pbc and Pb* indicate the common and radiogenic portions, respectively; 2) Error in standard calibration was 0.40% (not included in above errors but required when comparing data from different mounts); 3) Common Pb corrected using measured ^{204}Pb.

near but out of the crust–derived granites field in NW Zhejiang province as well as the crust–derived granites field in SE China (Fig. 10a), indicating that they cannot be formed only by the crust materials. Secondly, the Tongcun intrusive rocks have relatively high Mg# values from 35.40 to 40.30 and plot above the curve of pure crustal partial melt in Mg# vs. SiO_2 diagram (Fig. 10c), indicating they cannot be generated only by the melts from the basaltic lower continental crust but support the indispensable involvement of a mantle component (Rapp and Watson, 1995). Thirdly, the Pb isotopes of the Tongcun granitoids are distributed near the orogenic Pb evolution curve and different from the Middle–Late crust–derived intrusions (Fig. 11a and b), also suggesting that the Tongcun granitoids were derived from the mixing of mantle and crustal materials. Their $\varepsilon_{Nd}(t)$ values also support the involvement of a mantle component, e.g., their two–stage Nd model ages (1.46–1.54 Ga; Table 5) are significantly younger than those of basement metamorphic rocks in the Cathaysia Block (1.8–2.2 Ga; Chen et al., 1999) and close to the minimum boundary value of the east of Yangze Block (1.5–1.8 Ga Chen et al., 1999).

In the Tongcun granitoids, the 662–879 Ma inherited zircons (Table 2; Fig. 6b and Table 7) have the Th/U ratios varying from 0.42 to 1.61, which are higher than those of metamorphic zircons (the Th/U ratio is often ~0.01 or lower) (Rubatto, 2002; Hoskin and Schaltegger, 2003) and consistent with those of the magmatic origin (Belousova et al.,

2002). Moreover, Neoproterozoic igneous rocks as well as the coeval inherited zircons of magmatic origin with the ages of 700–1000 Ma have been widely reported in or near the east QHMB (Zhong et al., 2005; Wu et al., 2005a, 2005b, 2006; F.Y. Wu et al., 2007; R.X. Wu et al., 2007; Zheng et al., 2008; Bai et al., 2010; Zhou et al., 2014). Therefore, we propose that the Neoproterozoic igneous rocks (e.g., the basement rocks from the Shuanxiwu group) in the lower crust were mainly involved to form the parent magma of the Tongcun granitoids.

In $\varepsilon_{Nd}(t)$ vs. I_{Sr} diagram (Fig. 10a), the Tongcun granitoid samples plot between the basement rocks (represented by splite– and quartz–keratophyre in Pingshui Formation) and EM–II fields, and compared with end–members of DM, EM–I and HIMU in $^{206}Pb/^{204}Pb$ vs. I_{Sr} diagram (Fig. 10b), these samples are more close to the EM–II (Fig. 10b), as supported by the previous studies that the subcontinental lithospheric mantle of south China is EM–II type (Chung, 1999; Wang et al., 2008), suggesting that the Tongcun complex may be formed mainly by two end–members of the Shuangxiwu basement and the enriched lithospheric mantle.

6.3.3. Mechanism for generating the Tongcun intrusive complex

The Tongcun granitoids belongs to the high–K calc–alkaline I–type granites. Generally, there are four main interpretations regarding the origin of I–type granites, including: 1) advanced fractional crystallization

Table 3
Results of $^{40}Ar/^{39}Ar$ stepwise heating analysis for sericite of the Tongcun porphyry Mo-Cu deposit, northeast Zhejiang Province.

| T(°C)	$(^{40}Ar/^{39}Ar)_m$	$(^{36}Ar/^{39}Ar)_m$	$(^{37}Ar/^{39}Ar)_m$	^{40}Ar(%)	F	^{39}Ar ($\times 10^{-14}$ mol)	^{39}Ar (%)	Age(Ma)	±1σ
Sample weight = 24.8 mg, J = 0.00439									
600	17.9271	0.0013	0.2938	97.97	17.5667	1.67	2.98	134.34	0.68
670	19.6368	0.0013	0.2473	98.18	19.2825	3.19	5.70	146.94	0.72
730	20.3346	0.0009	0.0039	98.70	20.0705	6.07	10.82	152.70	0.74
790	20.7365	0.0009	0.0047	98.67	20.4607	7.12	12.70	155.54	0.75
850	20.8322	0.0009	0.0016	98.74	20.5703	9.00	16.06	156.34	0.75
910	20.8236	0.0009	0.0013	98.71	20.5553	10.69	19.07	156.23	0.75
970	20.9220	0.0013	0.0008	98.22	20.5497	8.83	15.75	156.19	0.75
1030	20.8977	0.0010	0.0011	98.52	20.5885	7.58	13.53	156.47	0.75
1150	20.8330	0.0011	0.0069	98.39	20.4969	1.66	2.95	155.81	0.80
1250	22.9081	0.0093	0.0501	87.98	20.1564	0.16	0.28	153.32	1.85
1450	42.4216	0.0727	0.8955	49.56	21.0390	0.08	0.14	159.75	4.86

F = $(^{40}Ar*/^{39}Ar)$; m: the measured isotopic ratios.
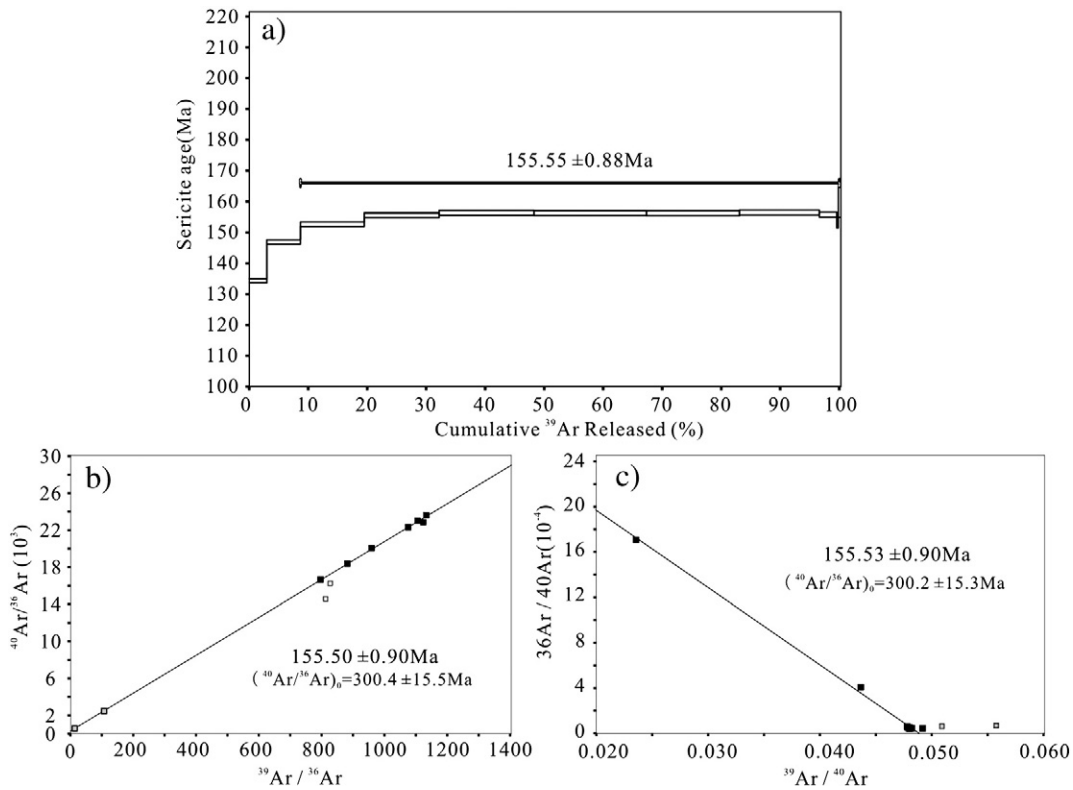
Fig. 7. Stepwise laser ablation analytical ^{39}Ar/^{40}Ar data for sericite. (a) Plateau age; (b) Normal isochron age; (c) Inverse isochron age.

of mantle–derived parental magmas, with or without crustal assimilation (DePaolo, 1981; Chiaradia, 2009; Li et al., 2004, 2009; El–Bialy and Omar, 2015); 2) partial melting of the lithospheric mantle, with or without being hybridized by the continental slab–derived melts (Altherr et al., 2000; Jiang et al., 2013a); 3) partial melting of infracrustal older igneous rocks or metamorphosed (metasedimentary) rocks (White and Chappell, 1977, 1983; Chappell and Stephens, 1988; Chappell and White, 1992, 2001; Altherr et al., 2000; Chappell et al., 2012; Huang et al., 2015; G.M. Li et al., 2015); 4) mixing of the melts from partial melting of supracrustal sedimentary rocks or remelting of pre–existing infracrustal igneous rocks and mantle–derived magmas (Gray, 1984; Barbarin, 1999; Griffin et al., 2002; Wu et al., 2003; Yang et al., 2004; Li et al., 2007b; Kemp et al., 2007; Li et al., 2009; Zhu et al., 2009; Liu et al., 2013; Xu et al., 2014; Wang et al., 2014; Guan et al., 2014). In this study, in the Harker diagrams (Fig. 13), most of the major and trace elements have no obvious liner correlation with increasing SiO_2. Moreover, they show the features of unfractional crystallization felsic granites in the Zr + Nb + Ce + Y versus FeO^T/MgO and $(K_2O + Na_2O)$ / CaO diagrams (Fig. 11c and d). Those characteristics may imply that fractional crystallization did not play a significant role during the formation process of the Tongcun granitoids. Integrating the features of magma sources discussed above, the Tongcun complex should be generated by mixing of the melts from partial melting or remelting of pre–existing Neoproterozoic igneous rocks and the melts from the enriched lithospheric mantle.

The Tongcun granitoids also show geochemical features of adakitic affinities. The characteristics, e.g., enrichment in LREE and depletion in HREE, and showing positive Rb, Th, U, Pb, Sr and negative Nb, Ta, Ti anomalies (Fig. 9), are consistent with those of a subduction component in the process of magma generation. However, their metaluminous nature, relatively low $\varepsilon_{Nd}(t)$ values of -6.3 to -7.3, high initial ^{87}Sr/^{86}Sr ratios of 0.70831–0.70904, enrichment in K_2O (Na_2O/K_2O = 0.88–1.25), positive Sr anomalies and no significant Eu anomalies, are obviously different from those of typical adakites, which formed by partial melting of the subducted oceanic slab (Defant and Drummond, 1990).

Actually, those intracontinental adakites, especially in east China, were considered to be derived from partial melting of mafic sections of the thickened lower continental crust, which previously underwent interaction with mantle material or underplating of mantle–derived basaltic melts at the base of the crust (Zhang et al., 2001; Hou et al., 2011, 2013; Berzina et al., 2014; B. Li et al., 2015). As showing in SiO_2 against Mg# and Th/Ce diagrams (Fig. 10c and d), the Tongcun granitoids plot in "Adakites related to lower crust melting with injecting of mantle material" and "Thick lower crust–derived adakitic rocks" fields, ruling out the derivation of partial melting of subducted oceanic slab melt (Defant and Drummond, 1990), the pure crust and delaminated lower crust (Stern and Hanson, 1991; Kay and Kay, 1993; Wang et al., 2006) as well as crustal assimilation and fractional crystallization (AFC) processes from parental basaltic magmas (Castillo et al., 1999). Considering that there was a thickened crust in the east China during the Jurassic to Cretaceous period due to the collision between the Eurasian and Paleo–Pacific plates (Deng et al., 2000, 2004), we propose that the Tongcun granitoids may be derived from partial melting of the thickened lower continental crust triggered by basaltic magma underplating plus additional input from the EM–II mantle derived basaltic melts. This mechanism is consistent with the fourth hypotheses above for the origin of I–type granites.

Based on these results above, we propose a simplified genetic model for the Tongcun granitoids, which is summarized as follows (Fig. 14): (1) during ~160 Ma, Tongcun area was controlled by an intracontinental compression setting, which was caused by the subduction from the Izanagi Plate to the Eurasian Plate; (2) intercontinental orogeny had occurred coevally, with the crust being thickened and the deep faults being activated; 3) the asthenospheric upwelling then triggered partial melting of the enriched lithospheric mantle which may be resulted from metasomatism by fluids derived from dehydration of a subducted slab; (4) larger amounts of basaltic magma derived from the enriched lithospheric mantle ascended to the base of the lower crust and triggered partial melting of crustal materials (mainly including the Neoproterozoic arc volcanic rocks in Shuanxiwu basement rocks). (5) crust–derived melts then mixed with the basaltic magmas,

Table 4
Major oxides (wt.%) and trace elements (ppm) for the Dayutang, Huangbaikeng granodiorites and the Xiatongcun monzogranite.

	KHB040	KHB041	KHB042	KHB043	KHB065–1	KHB065–2	KHB061	KHB060
Rock type	Dayutang granodiorite				Huangbaikeng granodiorite		Xiatongcun monzogranite, phase 1	
SiO_2	69.70	70.18	70.28	67.41	69.30	69.32	69.02	67.98
TiO_2	0.34	0.31	0.34	0.37	0.35	0.34	0.36	0.36
Al_2O_3	15.31	15.10	15.04	15.94	15.22	15.02	14.82	15.01
Fe_2O_{3T}	2.38	2.33	2.61	2.65	2.53	2.62	2.78	2.67
MnO	0.05	0.05	0.05	0.05	0.05	0.05	0.02	0.02
MgO	0.75	0.73	0.79	0.90	0.82	0.79	0.77	0.88
CaO	2.52	2.62	2.51	3.01	2.48	2.55	2.10	2.77
Na_2O	4.03	4.09	4.05	4.19	4.00	3.91	3.59	3.53
K_2O	3.43	3.69	3.53	3.36	3.56	3.67	4.10	4.03
P_2O_5	0.11	0.10	0.11	0.12	0.11	0.11	0.12	0.13
FeO	1.39	1.28	1.57	1.59	1.40	1.49	1.79	1.82
LOI	1.35	0.79	0.69	1.99	1.56	1.62	1.77	2.07
Total	99.96	99.99	99.99	99.99	99.97	99.99	99.45	99.45
Mg#	38.50	38.20	37.34	40.30	38.98	37.34	35.40	39.58
DI	80.59	81.41	80.66	77.51	80.48	80.33	81.36	78.61
Cr	4.90	4.65	5.33	5.90	8.45	7.09	7.14	6.48
Co	4.50	3.77	4.05	4.93	4.55	4.30	4.99	5.75
Ni	2.68	2.58	2.88	3.09	2.94	3.17	3.35	3.23
Rb	92.9	109	103	110	113	118	92.6	108
Sr	486	481	483	584	512	492	511	544
Ba	957	828	805	1018	1260	1096	1005	968
La	30.70	34.40	32.20	36.50	31.90	37.30	40.30	34.10
Ce	53.90	60.60	56.60	63.70	55.40	61.30	66.00	58.30
Pr	5.75	6.33	6.21	6.91	5.93	6.73	6.94	6.25
Nd	21.20	22.60	22.60	24.80	21.90	25.00	25.80	23.20
Sm	3.51	3.36	3.64	3.72	3.31	3.86	3.87	3.64
Eu	0.74	0.79	0.86	0.85	0.78	0.88	0.93	0.88
Gd	2.84	2.80	2.90	2.97	2.77	2.97	3.19	3.02
Tb	0.37	0.36	0.41	0.39	0.36	0.39	0.41	0.41
Dy	1.32	1.35	1.69	1.48	1.40	1.55	1.65	1.60
Ho	0.24	0.24	0.29	0.25	0.24	0.27	0.27	0.28
Er	0.60	0.69	0.82	0.73	0.68	0.71	0.74	0.75
Tm	0.10	0.10	0.13	0.11	0.11	0.11	0.10	0.11
Yb	0.59	0.63	0.77	0.66	0.60	0.64	0.66	0.65
Lu	0.08	0.09	0.10	0.09	0.09	0.09	0.09	0.09
Y	6.11	6.80	8.68	7.34	6.93	7.52	7.59	7.71
Zr	77.10	93.60	103.00	95.50	68.60	58.30	60.80	64.40
Hf	2.82	3.19	3.24	2.72	2.30	1.89	1.89	2.11
Nb	5.02	5.97	7.26	6.23	5.99	5.91	5.78	6.19
Ta	0.33	0.39	0.56	0.39	0.42	0.43	0.39	0.41
Th	11.20	13.20	14.00	11.20	11.80	13.70	13.20	11.60
U	3.33	3.96	5.03	3.40	2.74	3.28	2.87	2.55
Pb	25.60	26.40	25.60	18.40	24.20	25.90	18.90	17.60
δEu	0.70	0.76	0.78	0.75	0.77	0.77	0.78	0.79
ΣHREE	12.25	13.07	15.80	14.02	13.16	14.23	14.71	14.62
ΣREE	121.94	134.34	129.23	143.16	125.46	141.78	150.95	133.28
LREE/HREE	7.39	7.97	6.65	8.01	7.52	8.03	8.11	7.20
La_N/Yb_N	35.02	36.70	28.08	37.51	35.84	39.54	40.98	35.21
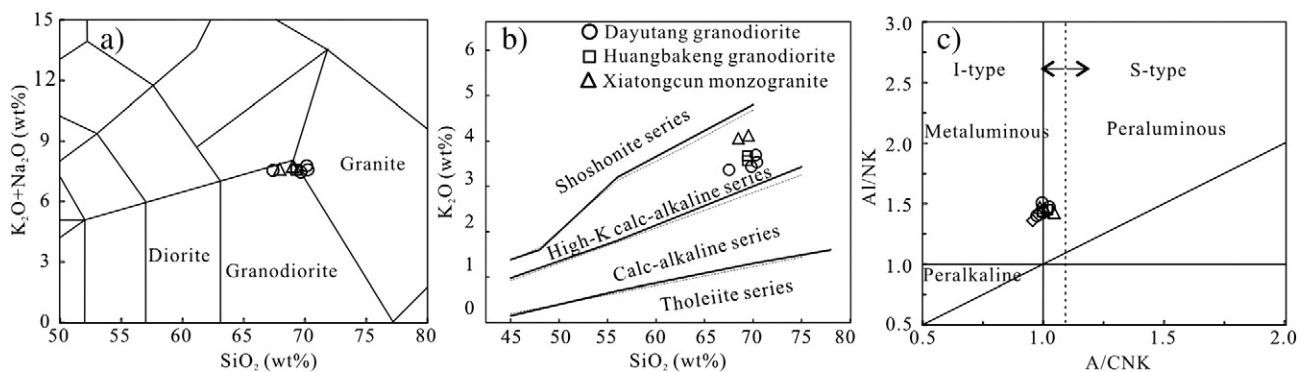
Fig. 8. (a) TAS classification diagram (Middlemost, 1994), (b) K_2O vs. SiO_2 diagram (solid lines from Peccerillo and Taylor, 1976; dashed lines from Middlemost, 1985) and (c) A/CNK vs. A/NK diagram (dashed line is based on Chappell and White, 1974) for the Tongcun intrusive complex.
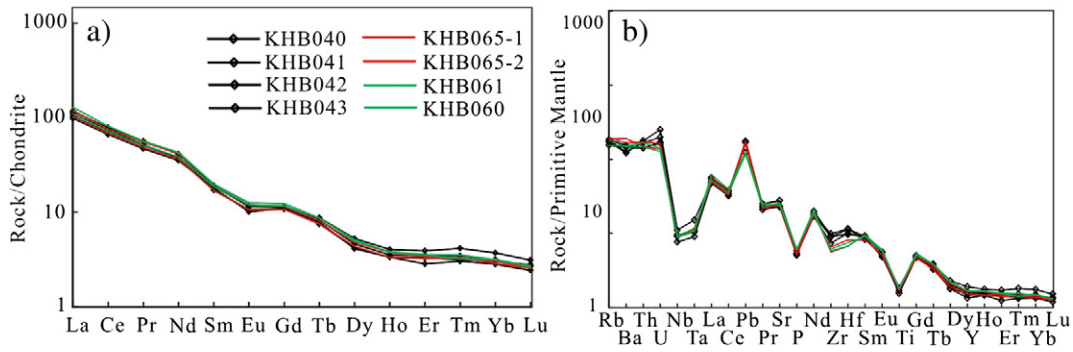
Fig. 9. Chondrite–normalized REE patterns and Primitive Mantle (PM) normalized trace element diagrams for three types of granitoids from the Tongcun intrusive complex. Chondrite and PM values are from Sun and McDonough (1989).

forming the Tongcun parental magmas; and (6) the parental magmas intruded the Cambrian and Ordovician sedimentary rocks along the NE trending faults and produced the Tongcun intrusive complex.

6.4. Implications for genesis of porphyry Mo–Cu deposits in collisional orogens

The genetic relationship between adakites or adakitic rocks and the porphyry Cu, Au deposits have been confirmed by many scholars in different tectonic settings, e.g., in arc settings, including the Los Pelambres giant porphyry copper deposit in the Andes (Reich et al., 2003) and most of porphyry Cu and epithermal Au deposits in the Philippines (Sajona and Maury, 1998) and in non–arc settings, including several significant porphyry Cu deposits in the eastern Tethyan metallogenic domain (Hou et al., 2011). Meanwhile, several porphyry Mo (Cu) deposits are also genetically associated with adakites or adakitic rocks, such as Yili porphyry Mo (Wu et al., 2015), the Shakhtama porphyry Mo–Cu (Berzina et al., 2013, 2014), the Aolunhua porphyry Mo–Cu (Ma et al., 2013) and the Tongchanggou porphyry–skarn type Mo–Cu deposits (Wang et al., 2014). Among them, the related adakites in Shakhtama porphyry Mo–Cu deposit show similarly geochemical characteristics with the Tongcun complex. Consequently, we believe that the Tongcun complex have close relationship with Mo–Cu mineralization, as also supported by following evidences.

1) Source of ore–forming materials and fluids

In this paper, molybdenite and chalcopyrite, which were collected from the early mineralization stage, have more enriched lead isotopic compositions than the Tongcun intrusive complex (Table 7; Fig. 11a and b). In the Pb evolution curve of Zartman and Doe (1981) (Fig. 11a and b), all these samples plot between the upper crust and orogenic Pb evolution curve, and are closer to the latter. Meanwhile, the sulfides plot between the Tongcun intrusive complex and the Jurassic crus–derived intrusions, and one chalcopyrite overlaps the Jurassic crus–derived intrusions. These indicate that ore–forming metals of the Tongcun Mo–Cu deposit came from a mixed source of mantle and crust. Therefore, we interpret that the magma and wall rocks should provide the ore–forming metals for the Tongcun Mo–Cu deposit. Moreover, S–H–O isotopes were also analyzed and reported by Tang et al. (2015a). Sulfur isotopic compositions from three molybdenite and chalcopyrite samples range from + 1.6‰ to + 3.8‰, with an average value of + 2.8‰, showing magmatic origins. Additionally, the $\delta^{18}O_{SMOW}$ and δD_{SMOW} values of ore–forming fluid vary from + 5.6‰ to + 8.6‰ and from − 71.8‰ to − 88.9‰, respectively, indicating a primary magmatic fluid source.

2) Temporal and spatial relationship between the Tongcun intrusions and Mo–Cu mineralization

The conomically viable Mo (Cu) and Cu ore bodies are mainly found in or around the monzogranite in Jiangjunwu and Xiatongcun area (Fig. 2), indicating that the early Mo (Cu) and late Cu mineralization have a close spatial relationship with the monzogranite. Additionally, two ages of 162.2–163.9 Ma and 155.5 Ma for Mo (Cu) and the late Cu mineralization, respectively, are coincident with the zircon U–Pb ages of 159.9 Ma (Qiu et al., 2013) for monzogranite (phase 1), also indicating that the early Mo (Cu) and late Cu mineralization have a closely temporal relationship with this intrusion.

Therefore, we suggest that the Tongcun porphyry Mo–Cu deposit is genetically associated with the emplacement of the monzogranite (phase 1) among the several intrusions in the Tongcun complex.

6.5. Tectonic implications from the Tongcun I–type and adakitic granitoids

The main dynamic process of the Mesozoic strong tectonomagmatic activities and mineralization in Southeastern China has been argued for a long time. At least four tectonic models were proposed for the Middle–Late Mesozoic periods, including: 1) inland compression or an active continental–margin setting related to the subduction and collision of the Paleo–Pacific Plate in Mesozoic time (Shu et al., 2011; J.W. Mao et al., 2013; Li et al., 2013a, 2013b, 2014; Zheng et al., 2013; S.H. Jiang et al., 2013; He et al., 2015); 2) an extensional setting (Wang et al., 2004;

Table 5
Sr–Nd isotopic compositions for the granitic samples from the Tongcun intrusive complex.

Sample	Age (Ma)	Rb (ppm)	Sr (ppm)	$^{87}Rb/^{86}Sr$	$^{87}Sr/^{86}Sr$	$(^{87}Sr/^{86}Sr)_i$	Sm (ppm)	Nd (ppm)	$^{147}Sm/^{144}Nd$	$^{143}Nd/^{144}Nd$	$\varepsilon_{Nd}(t)$	T_{2DM} (Ga)
Dayutang granodiorite												
KHB041	160	119	490	0.7010	0.71005	0.70846	3.75	23.70	0.0954	0.512182	− 6.8	1.51
KHB043	160	118	591	0.5757	0.70962	0.70831	3.58	21.90	0.0987	0.512161	− 7.3	1.54
Huangbaikeng granodiorite												
KHB065–1	160	120	525	0.6623	0.71016	0.70865	3.20	20.60	0.0938	0.512187	− 6.7	1.49
Xiatongcun monzogranite, phase 1												
KHB061	160	106	532	0.5746	0.71054	0.70924	3.49	24.10	0.0876	0.51220	− 6.3	1.46
KHB060	160	114	545	0.6079	0.71042	0.70904	3.31	21.60	0.0927	0.512171	− 7.0	1.52

Table 6
Pb isotopic compositions for the sulfides and the granitic samples from the Tongcun intrusive complex.

Sample	Age (Ma)	Pb	Th	U	$^{206}Pb/^{204}Pb$	$^{207}Pb/^{204}Pb$	$^{208}Pb/^{204}Pb$	$(^{206}Pb/^{204}Pb)_{160}$	$(^{207}Pb/^{204}Pb)_{160}$	$(^{208}Pb/^{204}Pb)_{160}$
		ppm			The measured value			The correction value		
Dayutang granodiorite										
KHB040	160	25.60	11.20	3.33	18.422	15.618	38.679	18.183	15.606	38.423
KHB041	160	26.40	13.20	3.96	18.470	15.622	38.664	18.194	15.608	38.371
KHB042	160	25.60	14.00	5.03	18.476	15.614	38.682	18.114	15.596	38.361
KHB043	160	18.40	11.20	3.40	18.486	15.619	38.663	18.146	15.602	38.306
Huangbaikeng granodiorite										
KHB065–1	160	24.20	11.80	2.74	18.440	15.623	38.671	18.232	15.613	38.385
KHB065–2	160	25.90	13.70	3.28	18.448	15.610	38.644	18.215	15.599	38.334
Xiatongcun monzogranite, phase 1										
KHB061	160	18.90	13.20	2.87	18.543	15.635	38.775	18.263	15.621	38.365
KHB060	160	17.60	11.60	2.55	18.512	15.629	38.725	18.245	15.616	38.338

Sample	Stage		Mineral	$^{206}Pb/^{204}Pb$	$^{207}Pb/^{204}Pb$	$^{208}Pb/^{204}Pb$
KHB038	Early Mo–Cu mineralization		Molybdenite	18.342	15.589	38.374
KHB023	Early Mo–Cu mineralization		Chalcopyrite	18.349	15.612	38.473
KHB051	Early Mo–Cu mineralization		Molybdenite	18.358	15.594	38.396
KHB051	Early Mo–Cu mineralization		Chalcopyrite	18.427	15.651	38.650
KHB052	Early Mo–Cu mineralization		Molybdenite	18.314	15.598	38.404
KHB053	Early Mo–Cu mineralization		Chalcopyrite	18.412	15.618	38.457

Meng et al., 2012; Zhao et al., 2012; Huang et al., 2015; Deng et al., 2015), which was attributed to delamination or foundering of the lower crust induced by the flat–slab subduction of the Pacific plate (Li et al., 2007b; Meng et al., 2012; Zhao et al., 2012; Huang et al., 2015; Deng et al., 2015); 3) related to the Mesozoic super mantle plume activity in East Asia (Zhang, 2013a, 2013b); and 4) related to lithosphere thinning and upwelling of asthenospheric matter, which converged beneath the eastern China and adjacent areas by extrusion force from four directions (including the subduction of Pacific plate) (Yang et al., 2009;

Geng et al., 2012). In this study, the negative Nb, Ta, Ti, and P anomalies and enriched initial $^{87}Sr/^{86}Sr$ ratios of 0.7083–0.7092 of the Tongcun intrusive complex are consistent with those of the subduction–related magmatism (Wang et al., 2001; Spurlin et al., 2005; Zhu et al., 2015). Meanwhile, no coeval A–type granites were found in the Tongcun deposit, though some place of southeastern China was controlled by an extension setting during ~150 to ~165 Ma, as supported by A–type granites in this region (Li et al., 2007b; Jiang et al., 2008; Zhu et al., 2008; Shu et al., 2011; Zhao et al., 2012). Therefore, we believe that
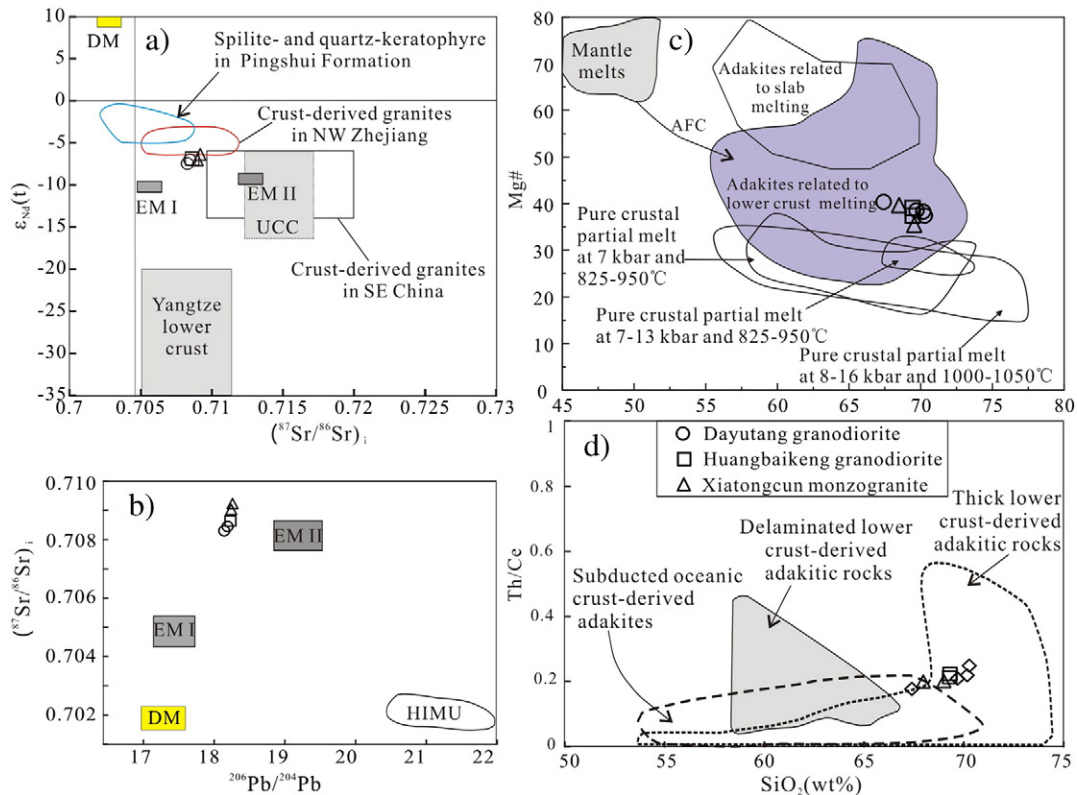
Fig. 10. Plots of I_{Sr} vs. $\varepsilon_{Nd}(t)$ (a), $^{206}Pb/^{204}Pb$ vs. I_{Sr} (b), SiO_2 vs. Mg# (c), SiO_2 vs. Th/Ce (d), and for three types of granitoids from the Tongcun intrusive complex. (The former two diagrams were modified from Li et al., 2013a; Wang et al., 2008, and the latter two were modified from Hou et al., 2013; Jiang et al., 2013b). Data of spilite– and quartz– keratophyre were from Shen et al. (1991), crust–derived intrusions of NW Zhejiang and SE China are from Li et al. (2013a, 2013b). DM: depleted mantle, EM I: enriched mantle I, EM II: enriched mantle II.
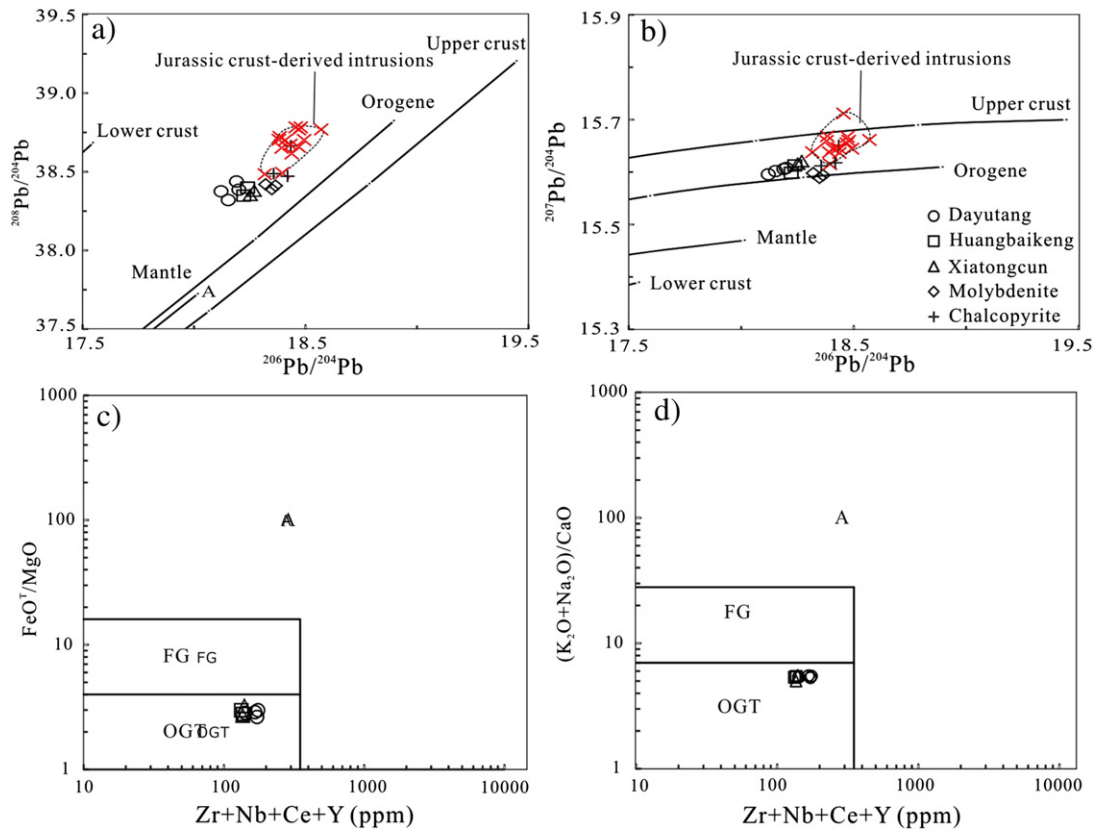
Fig. 11. Plots of $^{208}Pb/^{204}Pb$ vs. $^{206}Pb/^{204}Pb$ (a) and $^{207}Pb/^{204}Pb$ vs. $^{206}Pb/^{204}Pb$ (b) as well as $Zr + Nb + Ce + Y$ vs. FeO_T/MgO (c) and $(K_2O + Na_2O)/Ca_2O$ diagrams (d) for granitoids and sulfides from the Tongcun deposit (the data of Middle–Late Jurassic crust–derived intrusions of SE China are from S.H. Jiang et al., 2013; Li et al., 2013b). FG = Fractionated M–, I– and S–type felsic granites; OGT = unfractionated M–, I– and S–type granites.

the Tongcun intrusive complex formed in a compression setting related to the subduction of the Paleo–Pacific Plate in Mesozoic period.

7. Conclusions

1) The Tongcun intrusive complex mainly consists of granodiorite and monzogranite (phase 1 and 2) in Huangbaikeng, Dayutang, Jiangjunwu and Xiatongcun area, with the main emplacement ages varying from 160 Ma to 148 Ma. Three representative rock units from Tongcun intrusive complex are metaluminous to slightly peraluminous, and could be classified to high–K calc–alkaline I–type and adatikitic granitoids.

2) In the Tongcun Mo–Cu deposit, the late Cu mineralization event occurred at ~155.5 Ma. The early Mo (Cu) and late Cu mineralization events are temporally, spatially and genetically associated with the emplacement of monzogranite (phase 1).

3) The Tongcun intrusive complex was mainly derived from partial melting of the Neoproterozoic igneous rocks triggered by basaltic magma underplating plus additional input from the EM II mantle derived basaltic melts, and was totally controlled by a compression setting related to the subduction of the Paleo–Pacific plate in Mesozoic period.

Table 7
Zircons U–Pb dating from the previous studies of the Tongcun granitoids.

| Location	Rock type	U–Pb Method	Age (spots)	Th/U	Interpretation	Reference
Xiatongcun	Granite porphyry	SIMS	812 ± 50 (5) No CL photos	0.60–0.79	Trapped or Inherited zircons from Neoproterozoic igneous rocks	Zeng et al. (2013)
	Granite porphyry	LA–ICP–MS	155.6 ± 2.5(13) 164.8 ± 1.6 (13)		Crystallization age	Qiu et al. (2011)
	Granite porphyry	SHRIMP	662 ± 16(1) 797 ± 17(1)	0.56 and 0.64	Inherited zircons from Neoproterozoic igneous rocks	Zhu (2014)
Jiangjunwu	Granite porphyry	LA–ICP–MS	159.9 ± 3		Crystallization age	Qiu et al. (2013)
	Fine–grained granodiorite	SHRIMP	756 ± 17(1) 773 ± 18(1)	0.62 and 0.73	Inherited zircons from Neoproterozoic igneous rocks	Zhu (2014)
Huangbai–keng	Fine–grained granodiorite	SHRIMP	844 ± 15(1)	0.42	Inherited zircons from Neoproterozoic igneous rocks	Zhu (2014)
	Granodiorite	SHRIMP	648 ± 14(1) 703 ± 16(1)	1.11 and 1.61	Inherited zircons from Neoproterozoic igneous rocks	Zhu (2014)
	Fine–grained granite	SHRIMP	780.1 ± 2.8(1)	0.58	Inherited zircons from Neoproterozoic igneous rocks	Zhu (2014)
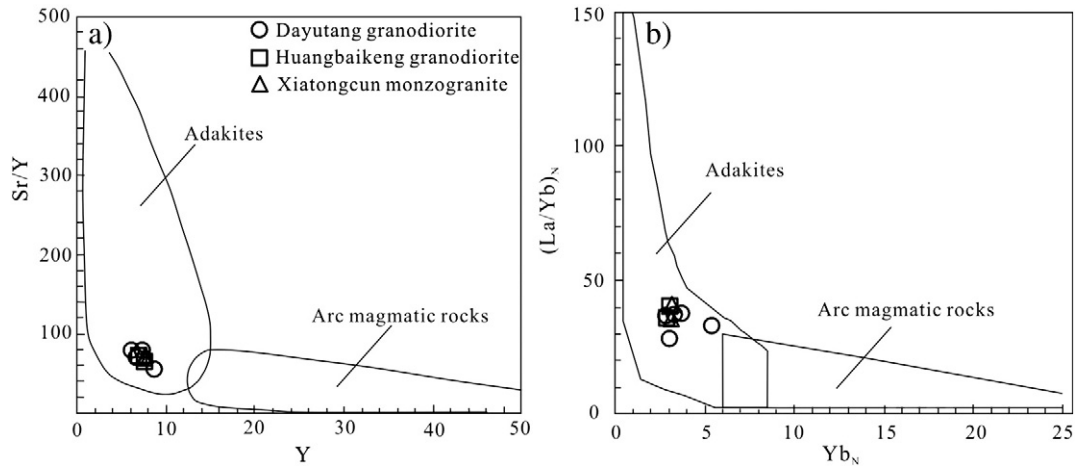
Fig. 12. Sr/Y vs.Y (a) and (La/Yb)$_N$ vs. Yb$_N$ (b) discrimination diagrams (after Defant and Drummond, 1990; Martin, 1986) for the Tongcun granitoids.
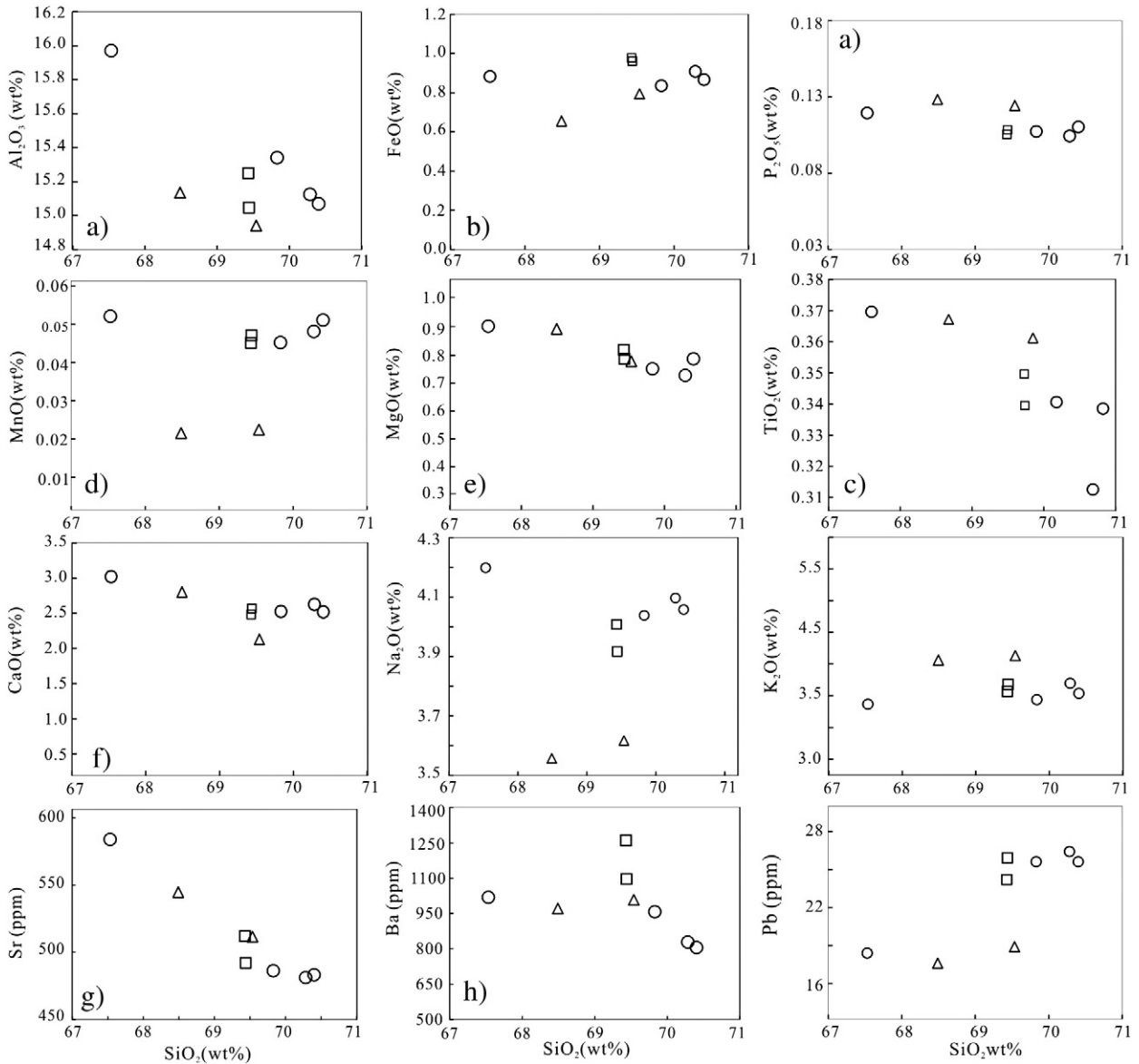

Fig. 13. Harker diagrams of SiO$_2$ against major elements and trace elements for the Tongcun granitoids.
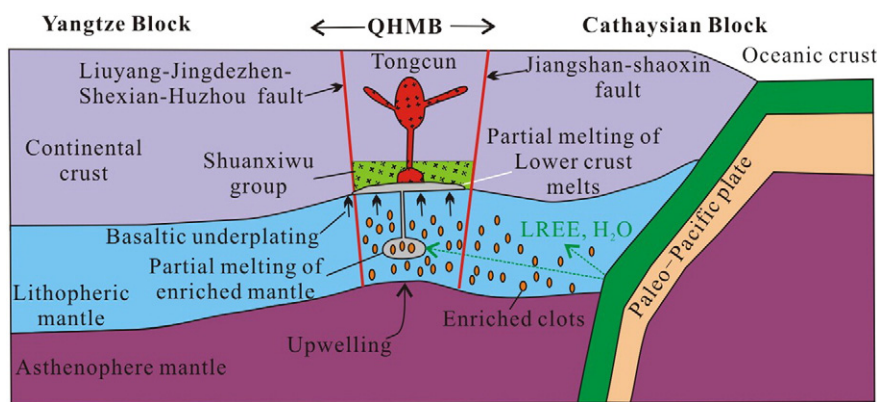
Fig. 14. Schematic illustrations of the generation and emplacement of the Tongcun intrusive complex. (Modified after Mao et al., 2011c; Liu et al., 2014.)

References

Altherr, R., Holl, A., Hegner, E., Langer, C., Kreuzer, H., 2000. High–potassium, calc–alkaline I–type plutonism in the European Variscides: northern Vosges (France) and northern Schwarzwald (Germany). Lithos 50, 51–73.

Atherton, M.P., Petford, N., 1993. Generation of sodium-rich magmas from newly underplated basaltic crust. Nature 362, 144–146.

Bai, D.Y., Jia, B.H., Liu, W., Chen, B.H., Liu, Y.R., Ghang, X.Y., 2010. Zircon SHRIMP U–Pb dating of the igneous rocks from Chengbu, Hunan: constraint on the Neoproterozoic tectonic evolution of the Jiangnan orogenic belt. Acta Geol. Sin. 84 (12), 1715–1726 (In Chinese with English abstract).

Baker, J., Peate, D., Waight, T., Meyzen, C., 2004. Pb isotopic analysis of standards and samples using a ^{207}Pb–^{204}Pb double spike and thallium to correct for mass bias with a double–focusing MC–ICP–MS. Chem. Geol. 211 (3–4), 275–303.

Barbarin, B., 1999. A review of the relationships between granitoid types, their origins and their geodynamic environments. Lithos 46, 605–626.

Belousova, E.A., Griffin, W.L., O'Reilly, S.Y., Fisher, N.I., 2002. Igneous zircon: trace element composition as an indicator of source rock type. Contrib. Mineral. Petrol. 143, 602–622.

Berzina, A.P., Berzina, A.N., Gimon, V.O., Krymskii, R.S., Larionov, A.N., Nikolaeva, I.V., Serov, P.A., 2013. The Shakhtama porphyry Mo ore-magmatic system (eastern Transbaikalia): age, sources, and genetic features. Russ. Geol. Geophys. 54 (6), 587–605.

Berzina, A.P., Berzina, A.N., Gimon, V.O., 2014. Geochemical and Sr–Pb–Nd isotopic characteristics of the Shakhtama porphyry Mo–Cu system (Eastern Transbaikalia, Russia). J. Asian Earth Sci. 79, 655–665.

BGMRZP (Bureau of Geology and Mineral Resources of Zhejiang Province), 1989g. Regional Geology of Zhejiang Province. People's Republic of China, Ministry of Geology and Mineral ResourcesGeological Memoirs, Series 1 No.11. Geological Publishing House, Beijing, pp. 519–526 (In Chinese).

Black, L.P., Kamo, S.L., Allen, C.M., Aleinikoff, J.N., Davis, D.W., Korsch, R.J., Foudoulis, C., 2004. TEMORA 1: a new zircon standard for Phanerozoic U–Pb geochronology. Chem. Geol. 200 (1–2), 155–170.

Castillo, P.R., Janney, P.E., Solidum, R.U., 1999. Petrology and geochemistry of Camiguin Island, southern Philippines: insights to the source of adakites and other lavas in a complex arc setting. Contrib. Mineral. Petrol. 134 (1), 33–51.

Chappell, B.W., Stephens, W.E., 1988. Origin of infracrustal (I–type) granite magmas. T. Roy. Soc. Edin-Earth 79, 71–86.

Chappell, B.W., White, A.J.R., 1974. Two contrasting granite types. Pac. Geol. 8, 173–174.

Chappell, B.W., White, A.J.R., 1992. I– and S–type granites in the Lachlan Fold Belt. T. Roy. Soc. Edin-Earth 83, 1–26.

Chappell, B.W., White, A.J.R., 2001. Two contrasting granite types: 25 years later. Aust. J. Earth Sci. 48, 489–499.

Chappell, B.W., Bryant, C.J., Wyborn, D., 2012. Peraluminous I–type granites. Lithos 153, 142–153.

Chen, S.Q., 2011. Discussion on the Yanshan Epoch Rock Characteristics and Ore–Forming Background in Zhejiang Kaihua Region. China University of Geosciences, pp. 18–40 (Paper for Master's Degree, In Chinese with English abstract).

Chen, B., Zhou, X.X., 2012. Ore-controlling factors and a metallogenic model for the Xianglushan tungsten-ore field in northern Jiangxi Province. Geol. Explor. 48, 0562–0569 (In Chinese with English abstract).

Chen, J.F., Guo, X.S., Tang, J.F., Zhou, T.X., 1999. Nd isotopic model ages: implications of the growth of the continental crust of southeastern China. J. Nanjing Univ. (Nat. Sci.) 35, 649–658 (in Chinese with English abstract).

Chen, F.K., Hegner, E., Todt, W., 2000. Zircon ages, Nd isotopic and chemical compositions of orthogneisses from the Black Forest, Germany: evidence for a Cambrian magmatic arc. Int. J. Earth Sci. 88, 791–802.

Chiaradia, M., 2009. Adakite–like magmas from fractional crystallization and melting–assimilation of mafic lower crust (Eocene Macuchi arc, western cordillera, Ecuador. Chem. Geol. 265, 468–487.

Chung, S.L., 1999. Trace element and isotope characteristics of Cenozoic basalts around the Tanlu fault with implications for the eastern plate boundary between North and South China. J. Geol. 107 (3), 301–312.

Composton, W., Williams, I.S., Mayer, C., 1984. U–Pb geochronology of zircons from lunar breccia 73217 using a sensitive high mass–resolution ion microprobe. J. Geophys. Res. 89, 525–534.

Compston, W., Williams, I.S., Kirschvink, J.L., Zhang, Z., Ma, G., 1992. Zircon U–Pb ages from the early Cambrian time–scale. J. Geol. Soc. 149, 171–184.

Defant, M.J., Drummond, M.S., 1990. Derivation of some modern arc magmas by melting of young subducted lithosphere. Nature 347, 662–665.

Deng, J.F., Zhao, G.C., Zhao, H.L., Luo, Z.H., Dai, S.Q., Li, K.M., 2000. Yanshanian igneous petrotectonic assemblage and orogenic–deep processes in east China. Geol. Rev. 46 (1), 41–48 (In Chinese with English abstract).

Deng, J.F., Luo, Z.H., Su, S.H., Mo, X.X., Yu, B.S., Lai, X.Y., Kan, H.W., 2004. Rock Genesis. Tectonic Settings and Metallogeny. Geological Publishing House, Beijing (380 pp., In Chinese with English abstract).

Deng, Y.F., Zhang, Z.J., Fan, W.M., Pérez-Gussinyé, M., 2015. Multitaper spectral method to estimate the elastic thickness of South China: implications for intracontinental deformation. Geos. Front. 5, 193–203.

DePaolo, D.J., 1981. A neodymium and strontium isotopic study of the Mesozoic calc–alkaline granitic batholiths of the Sierra–Nevada and Peninsular ranges, California. J. Geophys. Res. 86, 470–488.

Dong, S.W., Zhang, Y.Q., Long, C.X., Yang, Z.Y., Ji, Q., Wang, T., Hu, J.M., Chen, X.H., 2008. Jurassic tectonic revolution in China and new interpretation of the Yanshan movement. Acta Geol. Sin.-Engl. Ed. 82 (2), 334–347.

El–Bialy, M.Z., Omar, M.M., 2015. Spatial association of Neoproterozoic continental arc I–type and post-collision A–type granitoids in the Arabian–Nubian Shield: the Wadi Al–Baroud older and younger granites, north eastern desert, Egypt. J. Afr. Earth Sci. 103, 1–29.

Geng, S.F., Liu, P., Zheng, H.W., Wang, Z.Y., Ju, Y.J., 2012. A tentative discussion and new recognition of Mesozoic geodynamic mechanism in eastern China. Geol. Bull. China 31 (7), 1061–1068 (In Chinese with English Abstract).

Gray, C.M., 1984. An isotopic mixing model for the origin of granitic rocks in southeastern Australia. Earth Planet. Sci. Lett. 70, 47–60.

Griffin, W.L., Wang, X., Jackson, S.E., Pearson, N.J., O'Reilly, S.Y., Xu, X.S., Zhou, X.M., 2002. Zircon chemistry and magma mixing, SE China: in–situ analysis of Hf isotopes, Tonglu and Pingtan igneous complexes. Lithos 61, 237–269.

Gu, M.G., Feng, L.X., Hu, Y.H., Yu, S.Q., Wu, M., 2011. LA–ICP–MS U–Pb dating of zircons from Guangshan and Zhaxi plutons in Shaoxing area, Zhejiang Province: constraint on the ore–forming epoch of the Lizhu iron ore deposit. Geol. Bull. China 30 (8), 1212–1219 (In Chinese with English abstract).

Guan, Y.L., Yuan, C., Sun, M., Wilde, S., Long, X.P., Huang, X.L., Wang, Q., 2014. I–type granitoids in the eastern Yangtze Block: implications for the early Paleozoic intracontinental orogeny in South China. Lithos 206–207, 34–51.

Guo, S., Zhao, Y.Y., Qu, H.C., Wu, D.X., Xu, H., Li, C., Liu, Y., Zhu, X.Y., Wang, Z.K., 2012. Geological characteristics and ore-forming time of the Dexing porphyry copper ore mine in Jiangxi province. Acta Geol. Sin. (Engl. Ed.) 86, 691–899.

He, J.R., Wang, A.G., Rui, X.J., Li, C.H., 2005. Discussion on Mineralizing Process in East Integrating Zone of Qinzhou Bay and Hangzhou Bay. Earth Science Technology Forum of six Provinces and one Municipality in East China, 2005. Jiangsu Geological Institute, Nanjing, Jiangsu province, China, pp. 8–13 (In Chinese with English abstract).

He, G.J., Yang, X.C., Wu, G.M., Zhang, G.F., Cai, X.X., Zheng, J., 2011. A study of ore mineral characteristics and metallogenic stages of the Yinshan Ag–Pb–Zn polymetallic ore deposit, northwest Zhejiang province. Acta Geol. Sin. 32, 304–312 (In Chinese with English abstract).

He, C.S., Santosh, M., Dong, S.W., 2015. Continental dynamics of Eastern China: insights from tectonic history and receiver function analysis. Earth-Sci. Rev. 145, 9–24.

Hong, D.W., Xie, X.L., Zhang, J.S., 2002. Gological significance of the Hangzhou–Zhuguangshan–Huashan high-ε$_{Nd}$ granite belt. Geol. Bull. China 21 (6), 348–354 (In Chinese with English abstract).

Hoskin, P.W.O., Schaltegger, U., 2003. The composition of zircon and igneous and metamorphic petrogenesis. Rev. Mineral. Geochem. 53, 27–62.

Hou, Z., Zhang, H., Pan, X., Yang, Z., 2011. Porphyry Cu (–Mo–Au) deposits related to melting of thickened mafic lower crust: examples from the eastern Tethyan metallogenic domain. Ore Geol. Rev. 39 (1), 21–45.

Hou, Z., Pan, X., Li, Q., Yang, Z., Song, Y., 2013. The giant Dexing porphyry Cu–Mo–Au deposit in east China: product of melting of juvenile lower crust in an intracontinental setting. Miner. Deposita 48 (8), 1019–1045.

Hua, R.M., Chen, P.R., Zhang, W.L., Lu, J.J., 2005. Three major metallogenic events in Mesozoic in South China. Mineral deposits 11, 291–304 (In Chinese with English abstract).

Huang, H.Q., Li, X.H., Li, Z.X., Li, W.X., 2015. Formation of the Jurassic South China large granitic province: insights from the genesis of the Jiufeng pluton. Chem. Geol. 401, 43–58.

Jackson, S.E., Pearson, N.J., Griffin, W.L., Belousova, E.A., 2004. The application of laser ablation–inductively coupled plasma–mass spectrometry to in situ U–Pb zircon geochronology. Chem. Geol. 211 (1–2), 47–69.

Jia, S.H., Zhao, Y.Y., Wand, Z.Q., Wu, Y.D., Wand, T., Chen, L., 2014. Zircon U–Pb dating and geochemical characteristics of granodiorite–porphyry in the Linghou copper deposit, Western Zhejiang, and their geological significance. Acta Geol. Sin. 11 (88), 2071–2089 (In Chinese with English abstract).

Jiang, S.Y., Zhao, K.D., Jiang, Y.H., Dai, B.Z., 2008. Characteristics and genesis of Mesozoic A-type granites and associated mineral deposits in the Southern Hunan and Northern Guangxi provinces along the Shi-Hang Belt, South China. Geol. J. China Univ. 14 (4), 496–509 (In Chinese with English abstract).

Jiang, Y.H., Zhao, P., Zhou, Q., Liao, S.Y., Jin, G.D., 2011. Petrogenesis and tectonic implications of Early Cretaceous S- and A-type granites in the northwest of the Gan-Hang rift, SE China. Lithos 121, 55–73.

Jiang, S.H., Liang, Q.L., Bagas, L., Wang, S.H., Nie, F.J., Liu, Y.F., 2013. Geodynamic setting of the Zijinshan porphyry–epithermal Cu–Au–Mo–Ag ore system, SW Fujian province, China: constrains from the geochronology and geochemistry of the igneous rocks. Ore Geol. Rev. 53, 287–305.

Jiang, Y.H., Liu, Z., Jia, R.Y., Liao, S.Y., Zhou, Q., Zhao, P., 2013a. Miocene potassic granite–syenite association in western Tibetan Plateau: implications for shoshonitic and high Ba–Sr granite genesis. Lithos 134–135, 146–162.

Jiang, Y.H., Jia, R.Y., Liu, Z., Liao, S.Y., Zhao, P., Zhou, Q., 2013b. Origin of Middle Triassic high-K calc-alkaline granitoids and their potassic microgranular enclaves from the western Kunlun orogen, northwest China: a record of the closure of Paleo-Tethys. Lithos 156–159, 13–30.

Jin, W.S., Li, H.M., Que, Z.L., 2012. Geological characteristics and prospecting direction of Tongcun Cu–Mo deposit in Kaihua, Zhejiang province. Miner. Resour. Geol. 26 (5), 402–407 (In Chinese with English abstract).

Kay, R.W., Kay, S.M., 1993. Delamination and delamination magmatism. Tectonophysics 219, 177–189.

Kemp, A.I.S., Hawkesworth, C.J., Foster, G.L., Paterson, B.A., Woodhead, J.D., Hergt, J.M., Gray, C.M., Whitehouse, M.J., 2007. Magmatic and crustal differentiation history of granitic rocks from Hf–O isotopes in zircon. Science 315, 980–983.

Lee, J.Y., Marti, K., Severinghaus, J.P., Kawamura, K., Yoo, H.S., Lee, J.B., Kim, J.S., 2006. A re-determination of the isotopic abundances of atmospheric Ar. Geochim. Cosmochim. Acta 70, 4507–4512.

Li, Y.G., 2000. Qiantang–Qingfang old plate junction zone and its geological significance. Geol. Zhejiang 16, 17–24 (In Chinese with English abstract).

Li, B., Jiang, S.Y., 2014. Geochronology and geochemistry of Cretaceous Nanshanping alkaline rocks from the Zijinshan district in Fujian Province, South China: implications for crust–mantle interaction and lithospheric extension. J. Asian Earth Sci. 93, 253–274.

Li, X.H., Chung, S.L., Zhou, H.W., Lo, C.H., Liu, Y., Chen, C.H., 2004. Jurassic intraplate magmatism in southern Hunan–eastern Guangxi: ^{40}Ar/^{39}Ar dating, geochemistry, Sr–Nd isotopes and implications for the tectonic evolution of SE China. Geol. Soc. Lond., Spec. Publ. 226, 193–215.

Li, X.H., Li, W.X., Li, Z.X., 2007a. Re-discuss the genetic types and construct meaning of Early–Yanshan Epoch in Nanling. Chin. Sci. Bull. 52 (9), 981–991 (in Chinese).

Li, X.H., Li, Z.X., Li, W.X., Liu, Y., Yuan, C., Wei, G.J., Qi, C., 2007b. U–Pb zircon, geochemical and Sr–Nd–Hf isotopic constraints on age and origin of Jurassic I– and A–type granites from central Guangdong, SE China: a major igneous event in response to foundering of a subducted flat–slab? Lithos 96, 186–204.

Li, X.H., Li, W.X., Wang, X.C., Li, Q.L., Liu, Y., Tang, G.Q., 2009. Role of mantle–derived magma in genesis of early Yanshanian granites in the Nanling Range, South China: in situ zircon Hf–O isotopic constraints. Sci. China Ser. D Earth Sci. 52, 1262–1278.

Li, X.F., Xiao, R., Feng, Z.H., Wang, C.Y., Yang, F., Bai, Y.P., Jiang, S.K., Wang, Z.K., Zhu, X.Y., Xiao, N., Wei, X.L., 2011. Zircon SHRIMP U–Pb and Biotite Ar–Ar Ages from Fujiawu Porphyry Cu–Mo Deposit, Dexing, Southeast China: Implications for Magmatic–Hydrothermal Chronology. Let's Talk Ore Deposits vols. I and II, pp. 377–379.

Li, X.F., Hu, R.Z., Wei, X.L., Xiao, R., Xiao, N., Wang, C.Y., Yang, F., 2012. Mineral deposits types, mineralization features and genesis relationship between Jinshan gold deposit and Deixing porphyry copper deposit, northeastern Jiangxi province, South China. Geol. Rev. 58 (1), 82–90 (In Chinese with English abstract).

Li, Z.L., Zhou, J., Mao, J.R., Santosh, M., Yu, M.G., Li, Y.Q., Hu, Y.Z., Langmuir, C.H., Chen, Z.X., Cai, X.X., Hu, Y.H., 2013a. Zircon U–Pb geochronology and geochemistry of two episodes of granitoids from the northwestern Zhejiang Province, SE China: implication for magmatic evolution and tectonic transition. Lithos 179, 334–352.

Li, Z.L., Zhou, J., Mao, J.R., Yu, M.G., Li, Y.Q., Hu, Y.Z., Wang, H.H., 2013b. Age and geochemistry of the granitic porphyry from the northwestern Zhejiang Province, SE China, and its geological significance. Acta Petrol. Sin. 29 (10), 3607–3622 (In Chinese with English abstract).

Li, X.F., Watanabe, Y., Yi, X.K., 2013c. Ages and sources of ore-related porphyries at Yongping Cu–Mo deposit in Jiangxi province, southeast China. Resour. Geol. 63, 288–312.

Li, J.H., Zhang, Y.Q., Dong, S.W., Johnston, S.T., 2014. Cretaceous tectonic evolution of South China: a preliminary synthesis. Earth Sci. Rev. 134, 98–136.

Li, X.H., Liu, X.M., Liu, Y.S., Su, L., Sun, W.D., Huang, H.Q., Yi, K., 2015. Accuracy of LA–ICPMS zircon U–Pb age determination: an inter–laboratory comparison. Sci. China Earth Sci. 58, 1722–1730.

Li, G.M., Li, J.X., Zhao, J.X., Qin, K.Z., Cao, M.J., Evans, N.J., 2015. Petrogenesis and tectonic setting of Triassic granitoids in the Qiangtang terrane, central Tibet: Evidence from U–Pb ages, petrochemistry and Sr–Nd–Hf isotopes. J. Asian Earth Sci. 105, 443–455.

Li, B., Jiang, S.Y., Zhang, Q., Zhao, H.X., Zhao, K.D., 2015. Geochemistry, geochronology and Sr–Nd–Pb–Hf isotopic compositions of Middle to Late Jurassic syenite–granodiorites–dacite in South China: petrogenesis and tectonic implications. Gondwana Res.

Liu, L., Qiu, J.S., Li, Z., 2013. Origin of mafic microgranular enclaves (MMEs) and their host quartz monzonites from the Muchen pluton in Zhejiang Province, Southeast China: implications for magma mixing and crust–mantle interaction. Lithos 160–161, 145–163.

Liu, L., Qiu, J.S., Zhao, J.L., Yang, Z.L., 2014. Geochronological, geochemical, and Sr–Nd–Hf isotopic characteristics of Cretaceous monzonitic plutons in western Zhejiang Province, Southeast China: new insights into the petrogenesis of intermediate rocks. Lithos 196–197, 242–260.

Lu, S.D., Gao, W.L., Wang, S.L., Xiao, E., Xu, J.H., Liu, J., 2005. Pb isotopic compositions and its significance for ore genesis in Zhangshiba Pb–Zn deposit, Jiangxi. J. Mineral. Petrol. 25, 64–69 (In Chinese with English abstract).

Ludwig, K.R., 2003. Isoplot/Ex, Version 3: A Geochronological Toolkit for Microsoft Excel. Geochronology Center Berkeley, Berkeley. California.

Ma, X., Chen, B., Yang, M., 2013. Magma mixing origin for the Aolunhua porphyry related to Mo–Cu mineralization, eastern Central Asian Orogenic Belt. Gondwana Res. 24 (3), 1152–1171.

Mao, J.W., Xie, G.Q., Guo, C.L., Yuan, S.D., Cheng, Y.B., Chen, Y.C., 2008. Spatial-temporal distribution of Mesozoic ore deposits in South China and their metallogenic settings. Geol. J. China Univ. 14 (4), 510–526 (In Chinses with English abstract).

Mao, J.R., Yutaka, T., Li, Z.L., Takahashi, N., Ye, H.M., Zhao, X.L., Zhou, J., Hu, Q., Zeng, Q.T., 2009. Correlation of Meso-Cenozoic tectono- magmatism between SE China and Japan. Geol. Bull. China 28 (7), 844–856 (In Chinses with English abstract).

Mao, J.W., Chen, M.H., Yuan, S.D., Guo, C.L., 2011a. Geological characteristics of the Qinhang (or Shihang) metallogenic belt in South China and spatial– temporal distribution regularity of mineral deposits. Acta Geol. Sin. 85, 636–658 (In Chinese with English abstract).

Mao, J.W., Franco, P., Cook, N., 2011b. Mesozoic metallogeny in East China and corresponding geodynamic settings—an introduction to the special issue. Ore Geol. Rev. 43, 1–7.

Mao, J.W., Zhang, J.D., Pirajno, F., Ishiyama, D., Su, H.M., Guo, C.L., Chen, Y.C., 2011c. Porphyry Cu–Au–Mo–epithermal Ag–Pb–Zn–distal hydrothermal Au deposits in the Dexing area, Jiangxi province, East China—a linked ore system. Ore Geol. Rev. 43, 203–216.

Mao, J.W., Cheng, Y.B., Chen, M.H., Franco, P., 2013. Major types and time–space distribution of Mesozoic ore deposits in South China and their geodynamic settings. Mineral. Deposita 48, 267–294.

Mao, Z.H., Cheng, Y.B., Liu, J.J., Yuan, S.D., Wu, S.H., Xiang, X.K., Luo, X.H., 2013. Geology and molybdenite Re–Os age of the Dahutang granite–related veinlets–disseminated tungsten ore field in the Jiangxin Province, China. Ore Geol. Rev. 53, 422–433.

Martin, H., 1986. Effect of steeper Archean geothermal gradient on geochemistry of subduction-zone magmas. Geology 14, 753–756.

Meffre, S., Large, R.R., Scott, R., Woodhead, J., Chang, Z., Gilbert, S.E., Danyushevsky, L.V., Maslennikov, V., Hergt, J.M., 2008. Age and pyrite Pb–isotopic composition of the giant Sukhoi Log sediment–hosted gold deposit, Russia. Geochim. Cosmochim. Acta 72, 2377–2391.

Meng, L.F., Li, Z.X., Chen, H.L., Li, X.H., Wang, X.C., 2012. Geochronological and geochemical results from Mesozoic basalts in southern South China Block support the flat-slab subduction model. Lithos 132–133, 127–140.

Middlemost, E.A.K., 1985. Magma and Magmatic Rocks. Longman, London (266 pp.).

Middlemost, E.A.K., 1994. Naming materials in the magma/igneous rock system. Earth-Sci. Rev. 37, 215–224.

Nasdala, L., Hofmeister, W., Norberg, N., Mattinson, J.M., Corfu, F., Dörr, W., Kamo, S.L., Kennedy, A.K., Kronz, A., Reiners, P.W., Frei, D., Kosler, J., Wan, Y.S., Göze, J., Häer, T., Kröner, A., Valley, J.W., 2008. Zircon M257: a homogeneous natural reference material for the ion microprobe U–Pb analysis of zircon. Geostand. Geoanal. Res. 32, 247–265.

Paton, C., Woodhead, J.D., Hellstrom, J.C., Hergt, J.M., Greig, A., Maas, R., 2010. Improved laser ablation U–Pb zircon geochronology through robust down–hole fractionation correction. Geochem. Geophys. Geosyst. 11, 1525–2027.

Peccerillo, A., Taylor, D.R., 1976. Geochemistry of Eocene calc-alkaline volcanic rocks from the Kaitamonu area, Northern Turkey. Contrib. Mineral. Petrol. 58, 63–91.

Pei, R.F., 1995. Mineral deposit models of China. Beijing: Geological Publishing House, pp. 1–357 (In Chinese).

Qiu, J.T., Yu, X.Q., Zhang, D.H., Dai, Y.P., Li, H.K., Chen, S.Q., 2011. LA–ICP-MS zircon U–Pb dating of the Tongcun porphyry in Kaihua County, western Zhejiang Province, and its geological significance. Geol. Bull. China 30 (9), 1360–1368 (In Chinese with English abstract).

Qiu, J.T., Yu, X.Q., Santosh, M., Zhang, D.H., Chen, S.Q., Li, P.J., 2013. Geochronology and magmatic oxygen fugacity of the Tongcun molybdenum deposit, northwest Zhejiang, SE China. Mineral. Deposita 48, 545–556.

Rapp, R.P., Watson, E.B., 1995. Dehydration melting of metabasalt at 8–32 kbar: implications for continental growth and crust-mantle recycling. J. Petrol. 36 (4), 891–931.

Reich, M., Parada, M.A., Palacios, C., Dietrich, A., Schultz, F., Lehmann, B., 2003. Adakite-like signature of Late Miocene intrusions at the Los Pelambres giant porphyry copper deposit in the Andes of central Chile: metallogenic implications. Mineral. Deposita 38 (7), 876–885.

Richards, J.P., Kerrich, R., 2007. Special paper: adakite-like rocks: their diverse origins and questionable role in metallogenesis. Econ. Geol. 102 (4), 537–576.

Rubatto, D., 2002. Zircon trace element geochemistry: partitioning with garnet and the link between U–Pb ages and metamorphism. Chem. Geol. 184, 123–138.

Sack, P.J., Berry, R.F., Meffre, S., Falloon, T.J., Gemmell, J.B., Friedman, R.M., 2011. In situ location and U–Pb dating of small zircon grains in igneous rocks using laser ablation–inductively coupled plasma–quadrupole mass spectrometry. Geochem. Geophys. Geosyst. 12, Q0AA14.

Sajona, F.G., Maury, R.C., 1998. Association of adakites with gold and copper mineralization in the Philippines. C. R. Acad. Sci. IIA-Earth Planet. Sci. 326 (1), 27–34.

Seton, M., Müller, R.D., 2008. Reconstructing the Junction between Panthalassa and Tethys since the Early Cretaceous. PESA Eastern Australasian Basins Symposium III, Sydney, 14–17 September, pp. 263–266 (earthbyte.org).

Shen, W.Z., Zhang, B.T., Ling, H.F., Lai, M.Y., Yang, J.D., Tao, X.C., 1991. Nd, Sr and O isotopic study on spilite-keratophyre in Xiqiu, Zhejiang province. Acta Geol. Sin. 4, 337–346 (in Chinese with English abstract).

Shu, L.S., 2006. Predevonian tectonic is evolution of South China from Cathaysian Block to Caledonian period folded orogenic belt. Geol. J. China Univ. 12, 418–431 (In Chinese with English abstract).

Shu, L.S., Zhou, X.M., 2002. Late Mesozoic tectonism of Southeast China. Geol. Rev. 48 (3), 249–260 (in Chinese with English abstract).

Shu, X.J., Wang, X.L., Sun, T., Xu, X.S., Dai, M.N., 2011. Trace elements, U–Pb ages and Hf isotopes of zircons from Mesozoic granites in the western Nanling Range, South China: implications for petrogenesis and W–Sn mineralization. Lithos 127, 468–482.

Song, B., Zhang, Y.H., Wan, Y.S., Jian, P., 2002. Mount making and procedure of the SHRIMP dating. Geol. Rev. 48 (Suppl.), 26–30 (in Chinese).

Song, G.X., Qin, K.Z., Li, G.M., Evans, N.J., Li, X.H., 2014. Mesozoic magmatism and metallogeny in the Chizhou area, Middle–Lower Yangtze Valley, SE China: constrained by petrochemistry, geochemistry and geochronology. J. Asian Earth Sci. 91, 137–153.

Spurlin, M.S., Yin, A., Horton, B.K., Zhou, J., Wang, J., 2005. Structural evolution of the Yushu-Nangqian region and its relationship to syncollisional igneous activity, east-central Tibet. Geol. Soc. Am. Bull. 117 (9–10), 1293–1317.

Steiger, R.H., Jäger, E., 1977. Subcommission on geochronology: convention on the use of decay constants in geo– and cosmochronology. Earth Planet. Sci. Lett. 36, 359–362.

Stern, R.A., Hanson, G.N., 1991. Archean high-Mg granodiorite: a derivative of light rare earth element enriched monzodiorite of mantle origin. J. Petrol. 32 (1), 201–238.

Sun, S.S., McDonough, W.F., 1989. Chemical and isotopic systematics of oceanic basalts: implications for mantle composition and processes. Geol. Soc. Lond. Spec. Publ. 42 (1), 313–345.

Sun, M.D., Xu, Y.G., Wilde, S.A., Chen, H.L., Yang, S.F., 2015. The Permian Dongfanghong island-arc gabbro of the Wandashan orogen, NE China: implications for paleo-Pacific subduction. Tectonophysics 659, 122–136.

Tang, Y.W., Li, X.F., Xie, Y.L., Huang, C., Wei, H., Cai, J.L., Yin, Y.F., Qin, C.J., Liu, R., 2015a. Geology, geochemistry, and genesis of the Tongcun reduced porphyry Mo (Cu) deposit, NW Zhejiang Province, China. Acta Geol. Sin. (Engl. Ed.) 89 (3), 766–782.

Tang, Y.W., Li, X.F., Zhang, X.Q., Yang, J.L., Xie, Y.L., Lan, T.G., Huang, Y., Huang, C., Yin, R.C., 2015b. Some new data on the genesis of the Linghou Cu–Pb–Zn polymetallic deposit–based on the study of fluid inclusions and C–H–O–S–Pb isotopes. Ore Geol. Rev. 71, 248–262.

Thiéblemont, D., Stein, G., Lescuyer, J.L., 1997. Epithermal and porphyry deposits: the adakite connection. C. R. Acad. Sci. IIA-Earth Planet. Sci. 325 (2), 103–109.

Wang, L.L., 2010. The Alteration and Mineralization Characteristics and Geochemistry of Primary Halos of Porphyry Molybdenum (Copper) Deposit of Tongcun in Kaihua County of Zhejiang Province. China University of Geosciences, Beijing, pp. 1–78 (paper for master's degree, in Chinese with English abstract).

Wang, J.H., Yin, A., Harrison, T.M., Grove, M., Zhang, Y.Q., Xie, G.H., 2001. A tectonic model for Cenozoic igneous activities in the eastern Indo–Asian collision zone. Earth Planet. Sci. Lett. 188, 123–133.

Wang, Q., Zhao, Z.H., Jian, P., Xu, J.F., Bao, Z.W., Ma, J.L., 2004. SHRIMP zircon geochronology and Nd–Sr isotopic geochemistry of the Dexing granodiorite porphyries. Acta Petrol. Sin. 20, 315–324 (In Chinese with English abstract).

Wang, Q., Xu, J.F., Jian, P., Bao, Z.W., Zhao, Z.H., Li, C.F., Xiong, X.L., Ma, J.L., 2006. Petrogenesis of adakitic porphyries in an extensional tectonic setting, Dexing, South China: implications for the genesis of porphyry copper mineralization. J. Petrol. 47 (1), 119–144.

Wang, Y.J., Fan, W.M., Cawood, P.A., Li, S.Z., 2008. Sr–Nd–Pb isotopic constraints on multiple mantle domains for Mesozoic mafic rocks beneath the South China Block hinterland. Lithos 106, 297–308.

Wang, G.G., Ni, P., Zhao, K.D., Liu, J.R., Xie, G.A., Xu, J.H., Zhang, Z.H., 2011. Comparison of fluid inclusions in coexisting sphalerite and quartz from Yinshan deposit, Dexing, Northeast Jiangxi Province. Acta Petrol. Sin. 27, 1387–1397 (In Chinese with English abstract).

Wang, C.Y., Li, X.F., Xiao, R., Bai, Y.P., Yang, F., Mao, W., Jiang, S.K., 2012. Elements mobilization of mineralized porphyry rocks during hydrothermal alteration at Zhushahong porphyry copper deposit, Dexing district, South China. Acta Petrol. Sin. 28, 3869–3886 (In Chinese with English abstract).

Wang, G.G., Ni, P., Wang, R.C., Zhao, K.D., Chen, H., Ding, J.Y., Zhao, C., Cai, Y.T., 2013. Geological, fluid inclusion and isotopic studies of the Yinshan Cu–Au–Pb–Zn–Ag deposit, South China: implications for ore genesis and exploration. J. Asian Earth Sci. 74, 343–360.

Wang, X.S., Hu, R.Z., Bi, X.W., Leng, C.B., Pan, L.C., Zhu, J.J., Chen, Y.W., 2014. Petrogenesis of late Cretaceous I-type granites in the southern Yidun Terrane: new constraints on the late Mesozoic tectonic evolution of the eastern Tibetan Plateau. Lithos 208–209, 202–219.

Wang, G.C., Jiang, Y.H., Liu, Z., Ni, C.Y., Qing, L., Zhang, Q., 2015. Elemental and Sr-Nd-Hf isotopic constraints on the origin of Late Jurassic adakitic granodiorite in central Fujian province, southeast China. Mineral. Petrol. 109 (4), 501–518.

Whalen, J.B., Currie, K.L., Chappell, B.W., 1987. A-type granites: geochemical characteristics, discrimination and petrogenesis. Contrib. Mineral. Petrol. 96, 407–419.

White, A.J.R., Chappell, B.W., 1977. Ultrametamorphism and granitoid genesis. Tectonophysics 43, 7–22.

White, A.J.R., Chappell, B.W., 1983. Granitoid types and their distribution in the Lachlan Fold Belt, southeastern Australia. Geol. Soc. Am. Mem. 159, 21–34.

Wiedenbeck, M., Alle, P., Corfu, F., Griffin, W.L., Meier, M., Oberli, F., Vonquadt, A., Roddick, J.C., Speigel, W., 1995. 3 natural zircon standards for U–Th–Pb, Lu–Hf, trace–element and REE analyses. Geostand. Newslett. 19, 1–23.

Williams, I.S., 1998. U–Th–Pb Geochronology by Ion Microprobe. In: McKibben, M.A., Shanks III, W.C., Ridley, W.I. (Eds.), Applications of Microanalytical Techniques to Understanding Mineralizing Processes. Society of Economic Geologists, Colorado, pp. 1–35.

Wu, F.Y., Ge, W.C., Sun, D.Y., Guo, C.L., 2003. Discussions on the lithospheric thinning in eastern China. Earth Sci. Front. 10 (3), 51–60 (in Chinese with English abstract).

Wu, R.X., Zheng, Y.F., Wu, Y.B., 2005a. Zircon U–Pb age, element and oxygen isotope geochemisty of Neoproterozoic granites at Shiershan in South Anhui Province. Geol. J. China Univ. 11 (3), 364–382 (in Chinese with English abstract).

Wu, R.X., Zheng, Y.F., Wu, Y.B., 2005b. Zircon U–Ph age, element and oxygen isotope geochemisty of Neoproterozoic granodiorites in South Anhui. Acta Petrol. Sin. 21 (3), 587–606 (in Chinese with English abstract).

Wu, R.X., Zheng, Y.F., Wu, Y.B., Zhao, Z.F., Zhang, S.B., Liu, X.M., Wu, F.Y., 2006. Reworking of juvenile crust: element and isotope evidence from Neoproterozoic granodiorite in South China. Precambrian Res. 146, 179–212.

Wu, F.Y., Li, X.H., Yang, J.H., Zheng, Y.F., 2007. Discussions on the petrogenesis of granites. Acta Petrol. Sin. 23 (6), 1217–1238 (in Chinese with English abstract).

Wu, R.X., Zheng, Y.F., Wu, Y.B., 2007. Zircon U–Pb age and isotope geochemistry of Neoproterozoic Jingtan volcanics in South Anhui. Geol. J. China Univ. 13 (2), 282–296 (in Chinese with English abstract).

Wu, C., Jiang, T., Liu, W., Zhang, D., Zhou, Z., 2015. Early Cretaceous adakitic granites and mineralization of the Yili porphyry Mo deposit in the Great Xing'an Range: implications for the geodynamic evolution of northeastern China. Int. Geol. Rev. 57 (9–10), 1152–1171.

Xiao, Q.H., Li, Y., Feng, Y.F., Qiu, R.Z., Zhang, Y., 2010. A preliminary study of the relationship between Mesozoic lithosphere evolution in eastern China and the subduction of the Pacific plate. Geol. China 37, 1092–1101 (In Chinese with English abstract).

Xie, Y.L., Tang, Y.W., Li, Y.X., Li, Y., Liu, B.S., Qiu, L.M., Zhang, X.X., Jiang, Y.C., 2012. Magmatic intrusive series and their implication for the ore prospecting in Anji exploration area, Zhejiang province. Acta Petrol. Sin. 28, 3334–3346 (In Chinese with English abstract).

Xu, H.J., Ma, C.Q., Zhao, J.H., Zhang, J.F., 2014. Magma mixing generated Triassic I–type granites in South China. J. Geol. 122 (3), 329–351.

Xu, D.M., Lin, Z.Y., Luo, X.Q., Zhang, K., Zhang, X.H., Huang, H., 2015. Metallogenetic series of major metallic deposits in the Qinzhou–Hangzhou metallogenic belt. Earth Sci. Front. 22 (2), 007–124 (In Chinese with English abstract).

Yang, M.G., Mei, Y.W., 1997. Characteristics of geology and metallization in the Qinzhou–Hangzhou paleoplate juncture. Geol. Miner. Resour. South China 52–59 (In Chinese with English abstract).

Yang, J.H., Wu, F.Y., Chung, S.L., Wilde, S.A., Chu, M.F., 2004. Multiple sources for the origin of granites: geochemical and Nd/Sr isotopic evidence from the Gudaoling granite and its mafic enclaves, northeast China. Geochim. Cosmochim. Acta 68, 4469–4483.

Yang, M.G., Huang, S.B., Lou, F.S., Tang, W.X., Mao, S.B., 2009. Lithospheric structure and large-scale metallogenic process in Southeast China continental area. Geol. China 36, 528–543 (In Chinese with English abstract).

Yang, S.Y., Jiang, S.Y., Zhao, K.D., Jiang, Y.H., Ling, H.F., Luo, L., 2012. Geochronology, geochemistry and tectonic significance of two Early Cretaceous A-type granites in the Gan-Hang Belt, Southeast China. Lithos 150, 155–170.

Zartman, R.E., Doe, B.R., 1981. Plumbotectonics—the model. Tectonophysics 75, 135–162.

Zeng, Q.D., Wang, Y.B., Zhang, S., Liu, J.M., Qin, K.Z., Yang, J.H., Sun, W.D., Qu, W.J., 2013. U–Pb and Re–Os geochronology of the Tongcun molybdenum deposit and Zhilingtou gold–silver deposit in Zhejiang Province, Southeast China, and its geological implications. Resour. Geol. 63, 99–109.

Zhang, Q., 2013a. Is the Mesozoic magmatism in eastern China related to the westward subduction of the Pacific plate? Acta Petrol. Mineral. 32 (1), 113–128 (In Chinese with English Abstract).

Zhang, Q., 2013b. A discussion on Mesozoic large scale magmatism and felsic large igneous province in eastern China. Acta Petrol. Mineral. 32 (4), 557–564 (In Chinese with English Abstract).

Zhang, Q., Qian, Q., Wang, E.Q., Wang, Y., Zhao, T.P., Hao, J., Guo, G.J., 2001. An east China plateau in mid-late Yanshanian period: implication from adakites. Chin. J. Geol. 36 (2), 248–255 (In Chinese with English abstract).

Zhang, S.M., Xiao, Y.F., Wang, Q., Zhang, X.H., Yang, L., Wang, Y.L., Zhang, C.M., 2013. Re–Os dating of molybdenite from the Tongcun porphyry molybdenum deposit in western Zhejiang Province and its geological implications. Geol. Explor. 49 (1), 0050–0057 (In Chinese with English abstract).

Zhao, K.D., Jiang, S.Y., Yang, S.Y., Dai, B.Z., Lu, J.J., 2012. Mineral chemistry, trace elements and Sr-Nd-Hf isotope geochemistry and petrogenesis of Cailing and Furong granites and mafic enclaves from the Qitianling batholith in the Shi-Hang zone, South China. Gondwana Res. 22, 310–324.

Zheng, Y.F., Wu, R.X., Wu, Y.B., Zhang, S.B., Yuan, H.L., Wu, F.Y., 2008. Rift melting of juvenile arc–derived crust: geochemical evidence from Neoproterozoic volcanic and granitic rocks in the Jiangnan orogen, South China. Precambrian Res. 163, 351–383.

Zheng, Y.F., Zhao, Z.F., Chen, Y.X., 2013. Continental subduction channel processes: plate interface interaction during continental collision. Chin. Sci. Bull. 58, 4371–4377.

Zhong, Y.F., Ma, C.Q., She, Z.B., Lin, G.C., Xu, H.J., Wang, R.J., Yang, K.G., Liu, Q., 2005. SHRIMP U–Pb zircon geochronology of the Jiuling granitic complex batholith in Jiangxi Province. J. Earth Sci. 30 (6), 685–691 (in Chinese with English abstract).

Zhou, X.M., Sun, T., Shen, W.Z., Shu, L.S., Niu, Y.L., 2006. Petrogenesis of Mesozoic granitoids and volcanic rocks in South China: a response to tectonic evolution. Episodes 29, 26–33.

Zhou, Q., Jiang, Y.H., Zhao, P., Liao, S.Y., Jin, G.D., 2012. Origin of the Dexing Cu-bearing porphyries, SE China: elemental and Sr–Nd–Pb–Hf isotopic constraints. Int. Geol. Rev. 54 (5), 572–592.

Zhou, J.B., Zheng, Y., Zeng, C.Y., Liang, J., 2014. Neoproterozoic Tectonic–Magmatic Evolution of the Jiangnan Orogenic Belt. Science Press, Beijing, China, pp. 10–11 (In Chinese).

Zhou, Y.Z., Zheng, Y., Zeng, C.Y., Liang, J., 2015. On the understanding of Qinzhou Bay–Hangzhou Bay metallogenic belt, south China. Earth Sci. Front. 22 (2), 001–006 (In Chinese with English abstract).

Zhu, Y.D., 2014. Diagenesis and Metallogeny of Ore–Bearing Granites in Tongcun Porphyry Mo–Cu Deposit, Zhejiang. China University of Geosciences, Beingjing, pp. 38–48 (paper for doctoral degree, In Chinese with English abstract).

Zhu, J.C., Chen, J., Wang, R.C., Lu, J.J., Xie, L., 2008. Early Yanshanian NE trending Sn/W-bearing A-type granites in the western–middle part of the Nanling Mts region. Geol. J. China Univ. 14 (4), 474–484 (in Chinese with English abstract).

Zhu, D.C., Mo, X.X., Wang, L.Q., Zhao, Z.D., Niu, Y.L., Zhou, C.Y., Yang, Y.H., 2009. Petrogenesis of highly fractionated I–type granites in the Chayu area of eastern Gangdese, Tibet: constraints from zircon U–Pb geochronology, geochemistry and Sr–Nd–Hf isotopes. Sci. China D Earth Sci. 39 (7), 833–848 (In Chinese with English abstract).

Zhu, Y.D., Ye, X.F., Zhang, D.H., Wang, K.Q., 2012. Comparative study of granites in Tongcun porphyry molybdenum–copper deposit in west of Zhejiang province and Dexing porphyry copper deposit. Adv. Earth Sci. 27 (10), 1043–1053 (In Chinese with English abstract).

Zhu, Y.D., Ye, X.F., Zhang, D.H., Wang, K.Q., Wang, C.S., Yin, X.B., 2014. Petrochemistry, SHRIMP dating and Sr–Nd isotopic constraints on the origin of the Kaihua porphyry Mo (Cu) deposit, Zhejiang Province. Earth Sci. Front. 21, 1–14 (in Chinese with English abstract).

Zhu, R.Z., Lai, S.C., Qin, J.F., Zhao, S.W., 2015. Early-Cretaceous highly fractionated I-type granites from the northern Tengchong block, western Yunnan, SW China: petrogenesis and tectonic implications. J. Asian Earth Sci. 100, 145–163.